Theses and Dissertations

2015

Finite Element Modeling of Impact-Generated Stress Wave Propagation in Concrete Plates for Non-Destructive Evaluation

Tripti Pradhan
Lehigh University

Follow this and additional works at: http://preserve.lehigh.edu/etd

Part of the Civil and Environmental Engineering Commons

Recommended Citation

Pradhan, Tripti, "Finite Element Modeling of Impact-Generated Stress Wave Propagation in Concrete Plates for Non-Destructive Evaluation" (2015). *Theses and Dissertations*. Paper 1597.

FINITE ELEMENT MODELING OF IMPACT-GENERATED STRESS WAVE PROPAGATION IN CONCRETE PLATES FOR NON-DESTRUCTIVE EVALUATION

By

Tripti Pradhan

A Thesis

Presented to the Graduate and Research Committee

of Lehigh University

in Candidacy for the Degree of

Master of Science

in

Civil and Environmental Engineering

Lehigh University

November 2014

This thesis is accepted and approved in partial fulfillment of the requirements for the

Master of Science in Structural Engineering.

_____

Date

_____

Professor Stephen Pessiki

_____

Dr. Wesley Keller

_____

Professor Panos Diplas

ii

ACKNOWLEDGMENTS

TABLE OF CONTENTS

v

LIST OF TABLES

LIST OF FIGURES

ix

x

ABSTRACT

Impact-echo (IE) is a widely accepted and applied non-destructive evaluation technique for quality control and defect characterization in concrete structures. IE is an acoustic method based on the propagation of impact-generated stress waves that are reflected by material defects or interfaces. Numerical simulations using finite element method (FEM) have been used to study the impact-echo response of structural component with complex geometry and boundary conditions.

The present study focuses on developing a modeling methodology to simulate stress wave propagation in concrete plates. The significant modeling parameters that influenced the wave propagation and behavior were identified based on the literature review. A set of thirteen simulations were run to study the effect of each parameter. Time histories were recorded at four different locations to represent the waveform in an IE test. Fast Fourier transform (FFT) using Matlab was performed to transform the time-domain displacement histories to frequency-domain amplitude spectra.

The impact of steel ball on concrete plate was modeled using a force-time function with amplitude F_{max} for a given duration t_c. A gradually increasing force-function such as a half-cycle sine cubed was used to reduce the high-frequency ringing observed due to an abruptly increasing force. Similarly, distributing the force over two or more nodes eliminated the localized deformation of the concrete plate surface.

1

The unwanted wave reflections from the mechanical boundaries of a semi-infinite deteriorated the displacement waveform and had an adverse effect on thickness-mode frequency f_T. Absorbing layer with increased damping (ALID) boundaries were used to effectively absorb these wave reflection and give a more accurate amplitude spectrum. By implementing these absorbing boundaries, a significant reduction in model and computation cost was achieved.

Wave reflections from the free edges are important when modeling stress wave propagation in bounded sections. The foundation layer approach, where the concrete plate is supported by a flexible foundation layer, was used for modeling bounded concrete plates.

The relative difference in the stiffness of concrete and foundation layer R_K dictated the dynamic response of the system which primarily vibrated in piston-mode. A higher value of R_K was useful in separating the piston-mode from the thickness-mode frequencies to obtain a more accurate spectrum. The relative difference in the plate and foundation layer impedances R_Z influenced the behavior of propagating wave at the interface. A high value of R_Z was used to increase the coefficient of reflection R of the interface such that most of the incident compression wave reflected back as tension wave in the concrete plate.

2

CHAPTER 1. INTRODUCTION

1.1 INTRODUCTION

Impact-echo (IE) is a method for non-destructive evaluation (NDE) of concrete structures based on the propagation and interaction of mechanical impact induced stress wave in the concrete medium. It has a wide range of application ranging from quality control (thickness measurement, grouting in tendon ducts, epoxy injected in surface opening cracks, etc.) to defect characterization (location, shape and size of voids, surface opening cracks, delaminations etc.) (Sansalone & Street, 1997). It has also been used to measure the early age mechanical properties (set time and strength gain) of concrete (Pessiki & Carino, 1988; Pessiki & Johnson, 1996; Pessiki & Rowe, 1997).

New technologies such as stack imaging of spectral amplitude based on impact-echo (SIBIE) (Ohtsu & Watanabe, 2002) and rapid data acquisition through multisensor (Zhang, et al., 2012) and contactless sensing (Oh, 2012) have been used to improve the process and quality of defect characterization using the IE method.

Various numerical techniques like finite difference time domain (FDTD) and finite element method (FEM) have been employed to simulate the impact-echo response of various concrete, reinforced, and composite structural components. These techniques are based on the fundamental theory of elastic stress-wave propagation in an infinite solid

3

and have been successfully applied over a wide range of sections with complex geometric and boundary constraints.

FE models built using ABAQUS were analyzed to study the stress wave propagation in semi-infinite and bounded concrete plates due to a short-duration transient load. The formulation of impact load, its distribution and location, and mechanical boundary conditions were identified as significant modeling parameters. A total of thirteen simulations were run to investigate the effect of each parameter on the wave propagation characteristics.

Half-cycle sine and half-cycle sine cubed formulations were used to represent the impact of a steel ball on concrete surface. This impact load was distributed firstly over a single node as a concentrated load and then over nine elements as pressure load. The impact was applied at three different sites I_1 (doubly symmetric), I_2 (singly asymmetric) and I_3 (doubly asymmetric).

To study the transient response of semi-infinite sections, absorbing layer with increased damping (ALID) was used to absorb the unwanted wave reflections from the mechanical clamped boundaries. This absorbing layer was implemented in the FE model by introducing a mass proportional Rayleigh damping coefficient C_M.

A foundation layer approach was used to model wave propagation in bounded concrete plates. Relative stiffness R_K and relative impedance R_Z of the concrete and foundation

4

layer were found to have significant influence on the dynamic property of the structure and the behavior of stress wave at the interface.

1.2 RESEARCH OBJECTIVES

This research is primarily aimed at developing a methodology for finite element (FE) modeling of impact-generated stress wave propagation in concrete. In order to achieve this research objective the following approach was used.

1. Perform an in-depth literature review of previous studies conducted on impact-echo tests on concrete plates and numerical modeling of stress wave propagation using finite element analysis.

2. Develop an efficient and accurate dynamic finite element (FE) simulation of mechanical wave based impact-echo method for semi-infinite and bounded concrete plates.

3. Identify influential modeling parameters that affect the wave propagation characteristics in the concrete medium and conduct parametric studies of the identified parameters.

4. Study different methods to eliminate transient wave reflection from the numerical boundary and apply one of the methods in the FE model.

5. Develop a Matlab code to transform the displacement time-histories recorded at various nodes to amplitude spectra in frequency domain.

6. Compare the results for different parametric studies and draw conclusions based on the waveforms and amplitude spectra.

5

1.3 SCOPE OF THE PROJECT

The report is organized into five different chapters (Chapters 2-6) that discusses the following topics.

1. Chapter 2 provides the necessary background knowledge on the theory of elastic stress wave propagation in a solid medium. The general methodology behind the impact-echo method is also briefly discussed.

2. Chapter 3 provides the background for the numerical simulation of the stress wave propagation in concrete plate. The modeling of impact load, constraints on time step and element size, and the stability criteria of the time-stepping integration technique are covered. Modeling techniques for semi-infinite and bounded sections are discussed in detail.

3. Chapter 4 describes the finite element model used in this research. It also discusses the modeling parameters that were identified to significantly influence the wave propagation characteristics in the concrete plate.

4. Chapter 5 discusses the influence of the modeling parameters identified in Chapter 4. Time histories and amplitude spectra for each simulation case is discussed in detail.

5. Chapter 6 presents the summary and conclusions of the research work and proposes the future work that may be carried out to support the present findings.

6

1.4 SUMMARY OF FINDINGS

A set of thirteen simulations were run to study the effect of different parameters on the behavior of the propagating stress waves. The following findings were observed.

1. A high energy sudden impact (represented by half-cycle sine) yields a high frequency ringing in the waveform. This ringing effect can be eliminated by using a gradually increasing impact load (half-sine cubed).

2. Distributing the impact load over two or more nodes eliminates the undulations observed due to localized surface deformations due to a concentrated load.

3. Eccentric loading does not excite higher flexural modes in the assemblage other than the piston-mode frequency. However, the resulting waveform varies from that of symmetric loading case due to the early arrival of side reflections.

4. Non-reflecting and absorbing boundaries such as the absorbing layer with increased damping (ALID) can effectively absorb the boundary reflections in a semi-infinite sections. This greatly reduces the model size and the computational cost.

5. Modeling of bounded sections with complex boundaries, where side reflections are equally important, can be achieved by supporting the concrete on a foundation layer composed of different material properties (acoustic impedance). These properties dictate the behavior of propagating stress waves at the interface.

6. The foundation layer supporting the concrete slab behaves as a spring that vibrates in the piston-mode. This frequency can be easily identified in the respective amplitude spectrum.

7

The following notations were used in this report.

A	Cross-sectional area of plate/foundation layer
A_i	Amplitude of incident wave
$A_{reflected}$	Amplitude of reflected wave
$A_{refracted}$	Amplitude of refracted wave
C_K	Stiffness proportional Rayleigh damping coefficients
C_M	Mass proportional Rayleigh damping coefficients
C_P	Velocity of P-wave
C_R	Velocity of R-wave
C_S	Velocity of S-wave
$[C]$	Damping matrix
E	Young's modulus of elasticity
E_p	Elastic modulus of plate
E_s	Elastic modulus of steel ball
F_{max}	Amplitude of impact load

8

HS	Half-period sine
HSC	Half-period sine cubed
G	Shear modulus
K_f	Axial stiffness of the foundation layer
$[K]$	Stiffness matrix
L_D	Length of amplitude layer with increased damping (ALID)
$[M]$	Mass matrix
N	Mesh density per wavelength
R	Coefficient of reflection
R_K	Ratio of plate stiffness to foundation layer stiffness
R_Z	Ratio of plate impedance to foundation layer impedance
$\{R\}$	Vector of externally applied loads
T	Distance of the reflecting interface from the point of impact/thickness of concrete plate
T_f	Thickness of foundation layer
$\{U\}$	Displacement vector

$\{\dot{U}\}$	Velocity vector
$\{\ddot{U}\}$	Acceleration vector
Z	Acoustic impedance
Z_1	Acoustic impedance of material 1 from which the wave is propagating
Z_2	Acoustic impedance of material 2 into which the wave is propagating
m_c	Mass of concrete
m_s	Mass of steel ball
$f(t)$	Force-time function
f_T	Thickness mode frequency of plate of thickness T
f_{SDOF}	Fundamental frequency of SDOF approximation of plate-foundation layer assembly
f_P	Piston-mode frequency
f_{th}	Peak frequency corresponding to thickness-mode in the amplitude spectrum
g	Acceleration due to gravity
h	Drop height in (m)

10

n	Number of samples
r	Radius of steel ball (m)
t_c	Contact time of impact load
v_o	Velocity of the steel ball (m/s)
Δf	Frequency resolution
Δt	Sampling time / time increment
Δt_{cr}	Critical time increment
Δx	Element size
β	Correction factor
λ_{min}	Minimum wavelength
ν	Poisson's ratio
ν_p	Poisson's ratio of plate
ν_s	Poisson's ratio of steel ball
ρ	Material density
ξ_{max}	Fraction of critical damping in the mode with highest damping defined

11

ω_{max} Maximum cyclic frequency of impact load

ω_{SDOF} Cyclic frequency of SDOF system

CHAPTER 2. BACKGROUND

Impact-echo is a NDE method which utilizes propagating mechanical waves to determine the subsurface conditions. This chapter provides relevant information that is required to develop a basis for understanding the methodology of the impact-echo technique. A brief review on the elastic stress waves and its propagation in an infinite solid plate that defines the working principle of IE method is also provided. The stress waves propagating in a layered media and its behavioral characteristics at an interface of two dissimilar media is also briefly discussed.

Various studies exploring the numerical simulation of a solid concrete plate subjected to transverse elastic impact to form the basis of impact-echo method has been carried out in the past. Background information related to numerical modeling of wave propagation is separately provided in Chapter 3.

2.1   ELASTIC STRESS WAVES IN SOLIDS

The linear deformation in a solid body under the action of a short-period transient force at the surface (e.g. an impact of steel sphere on concrete surface) can be viewed as propagation of stress waves. Lamb studied the propagation of these stress waves due to an impulse at the surface of a half space (Lamb, 1904) and solid plate (Lamb, 1917).

13

Wave propagation theory has been widely used to study various geometric and loading situations (Rayleigh, 1888; Miklowitz, 1984; Graff, 1975).

Body waves and surface waves are the two types of waves propagating in a solid medium. Body waves (P-waves and S-waves) exists in an infinite medium and are undisturbed by the material boundaries or deformations. Surface waves (R-waves) travel along the surface of the medium. Figure 2.1 is the schematic representation of wave propagation and particle motion of P-, S- and R- stress waves in a solid half-space.

The P- or primary waves are longitudinal or dilatational waves which causes the particle to oscillate in the direction of wave propagation. These waves cause compressive and tensile stresses in the medium. The particle motion of the wavefront is in outward direction during the compression phase and in inward direction during the tension phase.

The S- or secondary waves are transverse or distortional waves causing the particle to oscillate in the direction perpendicular to the wave propagation direction. These waves produce shear stress in the medium and do not diverge, and they obey the continuity equation for incompressible media.

Rayleigh or R-waves are the surface waves that propagate along the surface or interface of a solid medium. These waves cause the particle to move in elliptical manner such that the surface appears to be moving in up and down motion. The amplitude of the wave decreases exponentially with increasing depth from the point of impact (Brekhovskikh, 2012)

14

2.1.1   Energy and Velocity of Stress Waves

The displacement field and radiation pattern of stress waves in solid plate was investigated by Miller and Pursey (Miller & Pursey, 1954). The R-waves have the largest amount of wave energy about 67 % of the total impact energy. The wave energy of P-wave is 7 % and that of S-wave is 26 % (Miller & Pursey, 1955). Figure 2.2 shows the displacement and energy distribution of stress waves due to a harmonic point source (Woods, 1968). The displacements due to P-waves have maximum amplitude directly beneath the source of impact whereas the amplitude of displacement due to S-waves is negligible around the area.

The velocity of the propagating stress wave in an infinite isotropic elastic medium is dependent on the material properties of the medium (Timoshenko, Goodier, & Abramson, 1970). P-wave travels at the highest speed in a solid medium with a velocity C_P given by Equation 2.1. S-wave also referred to as secondary waves is the second wave to arrive travelling at a velocity C_S given by the Equation 2.2. Rayleigh wave propagates the slowest among the three waves at a velocity C_R given by Equation 2.3 (Viktorov, 1967).

$$C_P = \sqrt{\frac{E(1-\nu)}{\rho(1+\nu)(1-2\nu)}} \qquad\qquad \textbf{2.1}$$

$$C_S = \sqrt{\frac{E}{2\rho(1+\nu)}} = \sqrt{\frac{G}{\rho}} \qquad\qquad \textbf{2.2}$$

$$C_R = \frac{0.87 + 1.12\nu}{1+\nu} C_S \qquad\qquad \textbf{2.3}$$

15

2.1.2 Behavior of Stress waves in Layers and Interfaces

Various studies have been conducted to investigate the behavior of wave propagation between layers by implementing appropriate boundaries (Brekhovskikh, 2012; Thomson, 1950). Concrete plates behave as a medium bounded by free boundaries on either side. The propagating stress waves are guided in the medium and refract, reflect or undergo mode conversion fulfilling the Snell's law at these boundaries. Figure 2.3 shows that a P-wave incident at free boundary gets transmitted as P-wave and SV-wave (the particle motion and direction of propagation occur in a vertical plane).

An interface is defined as the boundary between two dissimilar materials with different acoustic impedance properties. Acoustic impedance Z is the property of material defined as the product of P-wave speed C_P and density ρ of the medium. The relative difference in the acoustic impedances of the two materials constituting the interface dictates the behavior of the propagating P-waves.

The amplitudes of the reflected $A_{reflected}$ and the refracted $A_{refracted}$ waves depends upon the relative difference in the acoustic impedances between the two regions separated by the interface. These amplitudes are given by Equations 2.4 and 2.5 for an incident P-wave with amplitude A_i, propagating from material 1 with impedance Z_1 into material 2 with impedance Z_2. The ratio of the amplitude of reflection to the amplitude of refraction is termed as coefficient of reflection R and is simplified as Equation 2.6.

16

$$A_{reflected} = A_i \frac{Z_2 - Z_1}{Z_2 + Z_1} \qquad\qquad \textbf{2.4}$$

$$A_{refracted} = A_i \frac{2Z_2}{Z_2 + Z_1} \qquad\qquad \textbf{2.5}$$

$$R = \frac{Z_2 - Z_1}{Z_2 + Z_1} \qquad\qquad \textbf{2.6}$$

For the case when $Z_2 << Z_1$ (e.g. concrete/air) the amplitude of the refracted wave

approaches zero. The amplitude of reflected wave is equal to the amplitude of incident

wave and there occurs a phase change. This means that the incident compressive wave is

reflected back as a tension wave.

2.1.3 Scattering, Divergence and Attenuation

As the P-wave propagates in the solid medium, its wavefront spreads out therefore

decreasing the amplitude of the particle motion and the resulting displacement and

stresses. This condition occurs due to the phenomenon of divergence and attenuation.

Divergence is the spreading out of the stress wave wavefront as it propagates in a solid

medium. For non-planar waves, reduction in acoustic pressure also occurs due to

divergence. For a point source producing spherical wavefront, pressure wave vary as the

inverse of the path length due to phenomenon of divergence.

Scattering occurs as a result of reflection, refraction and mode conversion due to small

discontinuities within the medium or interfaces between dissimilar media. Attenuation on

17

the other hand takes place due to absorption and scattering of the wave. Internal friction and heat production leads to absorption of wave. In a heterogeneous medium like concrete, it affects the frequency content of the propagating pulse. The higher frequency components are attenuated with path lengths and the frequency spectrum of the pulse is continuously shifted to lower frequencies. Thus the sensitivity and the acoustic pressure decrease with path length.

2.2 IMPACT-ECHO METHOD

The impact-echo (IE) method was first developed by the joint efforts N. J. Carino and M. Sansalone (Sansalone & Carino, 1986; Carino, 2001) at the National Institute of Standards and Technology (NIST). Since then this method has been tested and applied for quality control and defect characterization of various plain, reinforced and post-tensioned concrete structures (Schubert, Wiggenhauser, & Lausch, 2004; Schubert & Köhler, 2008).

Figure 2.4 illustrates the principle and working of the IE method. The impact of steel sphere on the concrete surface generates elastic stress waves which propagate in the medium. The propagating waves are reflected by internal discrepancies or external boundaries. The surface displacements are measured by receiving transducer and analyzed in the frequency domain. The distance of the reflecting interface from the point of impact T is given by the Equation 2.7.

18

$$T = \frac{\beta C_P}{2f_{th}}$$

2.7

Where f_{th} is the peak frequency identified from the frequency spectrum and β is a factor related to shape of the section. For plates, a β factor of 0.96 was established (Sansalone, Streett, 1997). More recent study shows that β is related to the zero group velocity frequency of mode Lamb waves in a plate structure (Gibson & Popovics, 2005). A β value of 0.953 for poisson's ratio ν of 0.2 was adopted for present study.

2.2.1   Impact

During an impact (collision of steel sphere in the concrete surface) a portion of the potential energy in the sphere is transferred to the elastic wave energy in the plate which causes particle displacements. In the case of concrete, a mechanical impact source is normally used to generate a stress pulse with sufficient acoustic energy to overcome the effects of attenuation and divergence.

The impact theory proposed by Hertz has been studied to arrive at various mathematical formulations to accurately represent the force pulse (Hunter, 1957; McLaskey & Glaser, 2010). This pulse can be simplified as a force-time function consisting of a half-period sinusoidal force with maximum amplitude F_{max} for a duration of t_c (contact time).

For the purpose of this study two force-time functions: (a) Half-cycle Sine (HS), and (b) Half-cycle Sine Cubed (HSC) are considered to represent the impact load. Equation 2.8 and 2.9 represents the force-time function for the two impact cases.

19

HS $\qquad f(t) = F_{max} sin\left(\dfrac{\pi t}{t_c}\right)$ $\qquad$ **2.8**

HSC $\qquad f(t) = F_{max} sin^3\left(\dfrac{\pi t}{t_c}\right)$ $\qquad$ **2.9**

The contact time of an impact can be approximated by the Hertz elastic solution for a sphere dropped onto a thick plate as given by Equations 2.10 (Goldsmith, 1960). The amplitude of the impact force occurs at $t_c/2$ and is defined by Equation 2.11.

$$t_c = 0.00858 \frac{r}{h^{0.1}}$$ $\qquad$ **2.10**

$$F_{max} = \frac{1.140(v_o)^2 m_s}{\alpha_m}$$ $\qquad$ **2.11**

$$\alpha_m = \left(\frac{15\pi v_o^2}{16(r)^{0.5}}(\delta_s + \delta_p)m_s\right)^{0.4}$$

$$v_o = \sqrt{2gh}$$

$$m_s = \rho_s \frac{4}{3}\pi r^3$$

$$\delta_s = \frac{1 - v_s^2}{\pi E_s}$$

$$\delta_p = \frac{1 - v_p^2}{\pi E_p}$$

20

2.2.2 Waveforms

During an impact-echo test, the stress wave cause surface displacements which are captured by the transducer/recorder placed adjacent to the impact source. Analog voltage vs. time signal captured by the data acquisition (DAQ) system represents these surface displacements and is called waveform.

The waveform carries vital information about the structure in terms of the frequency produced by multiple reflection of P-wave at boundary and interfaces. The arrival of R-wave in the waveform causes a relatively large downward displacement and resembles an inverted half-sine wave, similar to the force-time function used to represent the impact.

For a concrete/air interfaces, the first and the subsequent odd multiples of reflected P-wave causes an outward displacement of the particle and are thus compression wave. The even multiples of the reflected P-waves are reflected as tension wave thus causing an inward displacement of the solid particle. These successive P-wave reflections excite a particular mode of vibration referred to as thickness mode. The frequency with which inward displacement occurs can be determined by taking the inverse of the time taken by the P-wave to travel twice the thickness of the plate with a velocity of C_P as shown in Equation 2.12.

$$f_T = \frac{\beta C_P}{2T} \qquad \textbf{2.12}$$

21

2.2.3 Frequency Domain Analysis

The time-domain waveform for an actual plate differs from that of an ideal plate and is complicated by the reflections of the S- and mode-converted P-waves. In such a case, it is difficult to identify the key thickness mode frequency directly from the waveform. For easy identification of the thickness frequency, the waveform is transformed to frequency domain to generate amplitude spectrum. The frequencies in an amplitude spectrum are well separated and the thickness frequency can be easily identified in terms of distinct peaks. In this study, amplitude spectra from the displacement-histories are obtained by implementing fast Fourier transform (FFT) using Matlab (Guide, 1998)

Frequency resolution Δf (Equation 2.13) is the frequency difference in discrete points in the amplitude spectrum and is the inverse of product of number of samples n and the sampling interval Δt. A high frequency resolution is desirable to capture all the key frequencies in the amplitude spectrum during an impact-echo test. A rule of thumb is to select a sampling frequency $(1/\Delta t)$ that is twice greater than the maximum frequency to be captured (Nyquist frequency).

$$\Delta f = \frac{1}{n\Delta t}$$

2.13

22
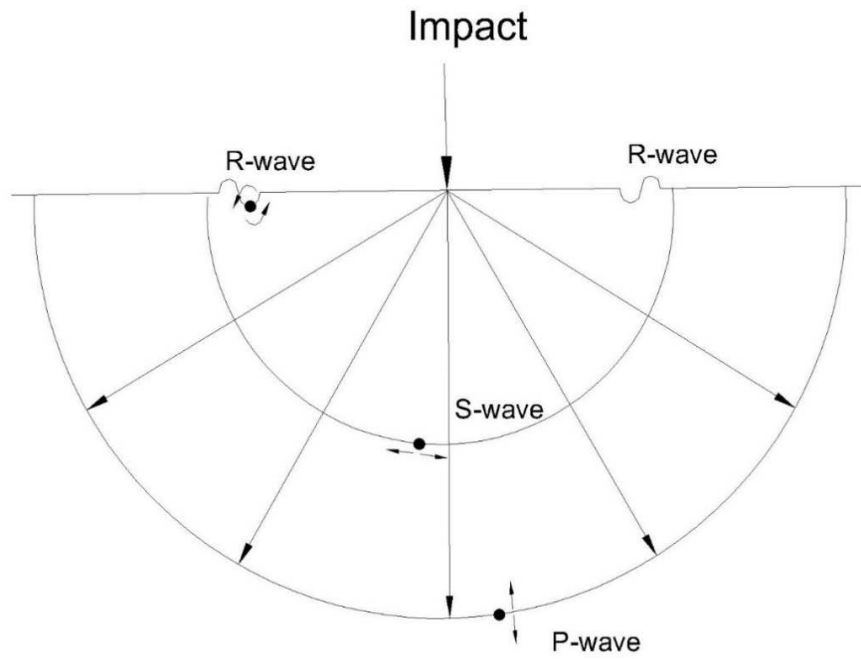
Figure 2.1   Wave propagation and particle motion of compressional, shear and Rayleigh waves.
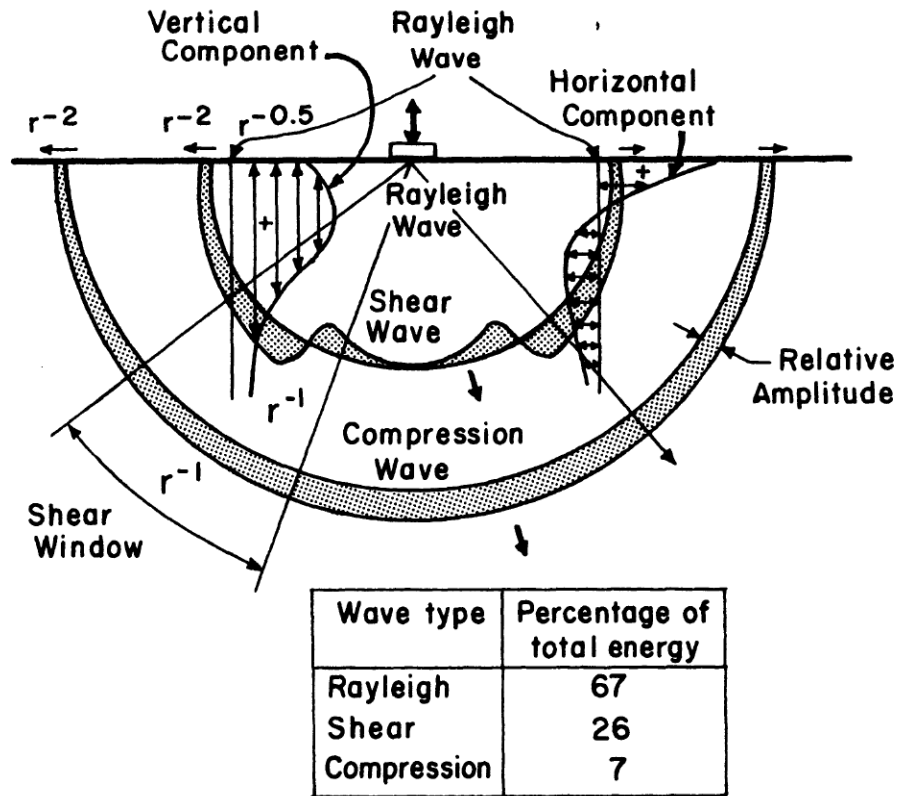
Figure 2.2   Schematic illustration of displacement and energy distribution of stress waves in a half-space due to harmonic normal load (Reproduced from Woods, 1968).

Wave type	Percentage of total energy
Rayleigh	67
Shear	26
Compression	7

24

$$\frac{\sin \theta}{c_{p1}} = \frac{\sin \beta}{c_{p2}} = \frac{\sin \theta_s}{c_{s1}} = \frac{\sin \beta_s}{c_{s2}}$$
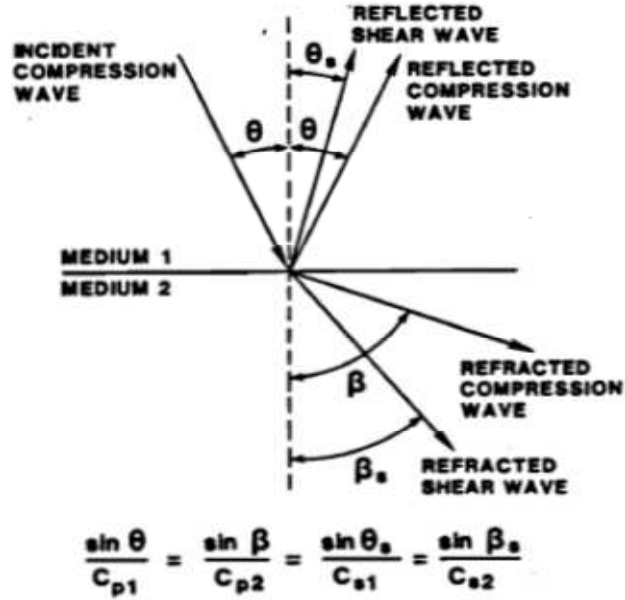
Figure 2.3   Behavior of P-wave incident upon an interface (Sansalone & Carino, 1986).

25
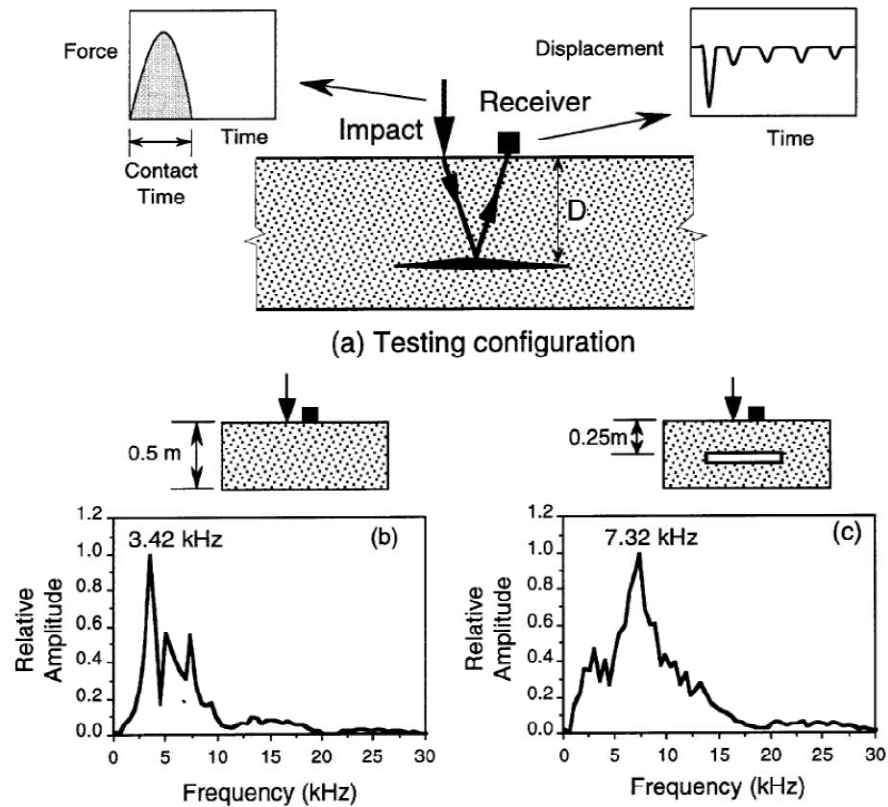
Figure 2.4 **Principle of impact-echo test. (a) Schematic of impact-echo method; (b) amplitude spectrum for test of solid slab; and (c) amplitude spectrum for test over void in slab (Davis, et al., 1998).**

26
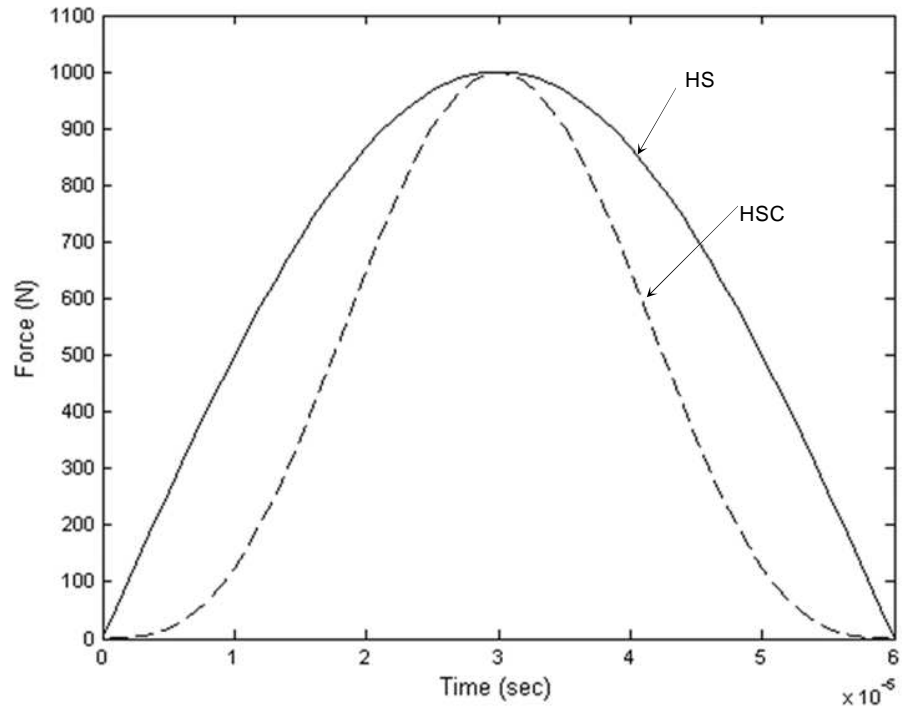
Figure 2.5   Representation of impact load by force-time function.

27

CHAPTER 3. FINITE ELEMENT MODELING OF IMPACT-ECHO TESTING

3.1 INTRODUCTION

Numerical methods such as finite-difference time-domain (FDTD) and finite element method (FEM) have been explicitly used to simulate stress wave propagation in solid medium (Chang & Randall, 1988; Ham & Bathe, 2012). These methods have been successfully applied to study the impact-echo response of concrete plates (Sansalone, Carino, & Hsu, 1987; Abramo, 2011).

This chapter provides relevant background on finite element (FE) modeling of stress wave propagation is concrete medium. The topics covered in this section forms the basis of the FE simulation and observed results discussed later in Chapter 4. The FEM consideration for impact load, element and time discretization, numerical integration algorithm and stability criteria are reviewed. Reflecting and absorbing boundary conditions for stress wave propagation in semi-infinite plate are discussed. To simulate the wave propagation in bounded solid, a new approach is proposed which makes used of a flexible foundation layer. Some of the techniques discussed in the subsequent sections are specific to the finite element analysis (FEA) software ABAQUS and may vary for a different FEA platform.

28

3.2 IMPACT LOAD

The impact of a steel ball on concrete surface can be numerically represented by the force-time function as discussed in Section 2.2.1. The amplitude of this force-time function F_{max} affects the magnitude of stresses and displacements that occur due to the stress waves generated by the impact. The value of F_{max} should be chosen such that induced deformations are under the linear elastic limit. The contact time t_c affects the cutoff frequency of the pulse and significantly influences the analytical result.

Figure 3.1(a) and (b) respectively show the force-time history and the amplitude spectrum for the two force functions discussed in Section 2.2.1. As observed the energy of the HS load is more than that of HSC load. Therefore HS would induce higher particle displacements than the HSC impact load. However the amplitude spectrum for the two load cases show that the maximum useful frequency is higher for the HSC case and covers broader range of excitation frequency.

As shown in Section 5.2 an impact load applied over a single node produces minute oscillations in the waveform which occurs as a result of localized deformation in the node. This effect can be eradicated completely by using two or more nodes to distribute the impact over a larger region.

29

3.3 ELEMENT TYPE

In the present study, three-dimensional models were built using ABAQUS/standard. First-order linear solid continuum elements (C3D8) were used to represent the concrete plate. The C3D8 element is an 8-node brick element with nodes only at the corners. The stresses/displacement at any intermediate location is obtained by linear interpolation between the corresponding corner nodes (ABAQUS, 2011).

Linear elements were used as the stresses/displacement caused by the propagating wave is very small and within the elastic range. For accurately representing the wave propagation problem, a very fine mesh is required to capture the wave traveling with wavelength $ë_{min}$. Full integration was chosen as opposed to reduced integration to avoid the excitation of any zero-energy mode or spurious-modes in the model.

3.4 SPATIAL AND TEMPORAL DISCRETIZATION

To avoid the errors associated with the numerical modeling of elastic wave propagation in a continuous medium, the discretization in time and space must be carefully chosen. The effective element length and the corresponding time step should be able to represent the complete wave travel accurately.

The element size Δx depends entirely upon the wavelength of the wave propagating through the element. It should be small enough to capture the wave with minimum wavelength λ_{min} and should not be so small that the wave crosses the element in one

30

wavelength. It is recommended that at least 10 elements per wavelength (N) should be

used for accurate modeling (Seron, Sanz, Kindelan, & Badal, 1990).

$$\Delta x = \frac{\lambda_{min}}{N} \qquad\qquad \textbf{3.1}$$

The time increment Δt can be calculated using the expression given by Equation 3.2,

where Δt_{cr} represents critical time increment. Time increment in a dynamic problem

also depends on the type of dynamic integration technique implemented in the analysis.

The limit on the temporal discretization based on the dynamic integration technique is

discussed below in Section 3.5.

$$\Delta t \leq \Delta_{tcr} \approx \frac{\Delta x}{C_P} \qquad\qquad \textbf{3.2}$$

3.5   NUMERICAL TIME-STEPPING METHODS FOR SIMULATING DYNAMIC RESPONSE

Stress wave propagation is a dynamic problem in which the response of the system varies

with time. Equation 3.3 gives the equilibrium equation governing the linear dynamic

response of system of finite elements (Bathe, 1996).

$$[M]\{\ddot{U}\} + [C]\{\dot{U}\} + [K]\{U\} = \{R\} \qquad\qquad \textbf{3.3}$$

Here, $[M]$ $[C]$ and $[K]$ are the mass, damping and stiffness matrix; $\{R\}$ is the vector of

externally applied loads; and $\{\ddot{U}\}$, $\{\dot{U}\}$, and $\{U\}$ are the response of the system

31

(acceleration, velocity and displacement respectively. Direct integration refers to the calculation of the response history step-by-step during which the integration satisfies the equilibrium equation at discrete time interval Δt.

3.5.1 Implicit vs. Explicit Algorithm

The type of dynamic integration scheme (implicit or explicit) used in FE procedures determines the size of element and the time increment used in the analysis. The criteria on which the integration schemes are compared are computational cost and numerical stability in arriving at an accurate solution of the problem.

In implicit schemes, the difference equations are combined with the equation of motion and the displacements are calculated directly by solving the governing equations. In the case of an implicit analysis, the mass $[M]$ and stiffness $[K]$ matrices are built for each time step. For a large number of elements and degrees of freedom, these matrices become quite large drastically increasing the computational time. An Implicit algorithm is unconditionally stable meaning that result is stable irrespective of Δt used however; the accuracy may be largely affected. Implicit analysis is more suitable for structural dynamics problem where the response is dominated by lower modes.

In an explicit formulation, the response quantities are expressed in terms of previously determined values of displacement, velocity and acceleration. Such methods do not require factorization of the stiffness and mass matrix in the step-by-step solution thus making it computationally more economical. However, an explicit algorithm is

32

conditionally stable meaning that the time increment Δt should not exceed the critical time step Δt_{cr} for the solution to converge. Explicit schemes are often more useful for wave propagation problems such as the one investigated in this project, where the high frequency modes are important.

3.5.2   Stability Analysis

When implementing an explicit algorithm in the dynamic analysis of stress wave propagation in concrete plate, care must be taken to meet the conditional stability criteria (Equation 3.4) imposed by the scheme. Here ω_{max} is the maximum cyclic frequency of the impact being applied on the concrete plate and ξ_{max} is the fraction of critical damping in the mode with highest damping defined by Equation 3.5. Here C_M and C_K are respectively the mass and stiffness proportional Rayleigh damping coefficients. For the models with absorbing layer with increased damping (ALID) the stability criteria reduces to Equation 3.6.

$$\Delta t \le \Delta t_{cr} = \frac{2}{\omega_{max}}\left(\sqrt{1 + {\xi_{max}}^2} - \xi_{max}\right) \qquad \textbf{3.4}$$

$$\xi_{max} = \frac{C_M}{2\omega_{max}} + \frac{\omega_{max}\,C_K}{2} \qquad \textbf{3.5}$$

$$\Delta t \le \Delta t_{cr} = \frac{2}{\omega_{max}}\left(\sqrt{1 + \left(\frac{C_M}{2\omega_{max}}\right)^2} - \frac{C_M}{2\omega_{max}}\right) \qquad \textbf{3.6}$$

33

3.6 NON-REFLECTING AND ABSORBING BOUNDARY CONDITIONS

The formulation of the IE method is based on the propagation of stress waves in an infinite solid medium (ideal plate). An ideal plate is a structure composed of two parallel surfaces, extending infinitely in the lateral direction. However, due to computational limitation of FEM only a finite length plate can be simulated in practice.

The Dirichlet and Neumann boundary conditions of the FE formulation possess the main challenge in the wave propagation simulation in a finite plate. The propagating waves are reflected by these boundary conditions which contaminates the recorded displacement histories. An easy way around is to build a model that is sufficiently large such that the boundary reflections do not reach the recorder location for the given analysis time. This however, makes the FE model extremely large and adds to the computational cost.

Various non-reflecting and absorbing boundaries have been proposed and applied to diminish the effect of boundary reflections. The Lysmer-Kuhlemeyer (LK) boundary is a non-reflecting boundary that uses a viscous damper with appropriate damping constant to absorb wave energy (Lysmer & Kuhlemeyer, 1969). The LK boundary is readily available in FEA software ABAQUS element library as "infinite elements" and can be easily implement in the model. However, it has been noted that these elements are only effective for normally incident and the value of damping cannot be adjusted (Oh, 2012).

The energy absorbing layer is another approach that suppresses the wave reflection by attenuating the outgoing waves. A perfectly matched layer (PML) is an absorbing

34

boundary in which the layer matches the impedance of the core area and absorbs the waves at all tangential angle of incidence (Berenger, 1994). Absorbing layer with increased damping (ALID) is an absorbing layer that uses Rayleigh damping to attenuate the amplitude of the propagating wave. Analytical models implementing PML and ALID absorbing boundaries significantly reduces the geometric and computational size of the numerical model (Drozdz, 2008). ALID is preferred in this study as it is easier to implement it in the FE package by using Rayleigh damping.

3.6.1   Absorbing Layer with Increased Damping

The absorbing layer with increasing damping (ALID) has the same basis as the LK boundaries. These layers are attached to the plate boundaries and the energy absorption is achieved by the means of viscous damping defined by mass proportional Rayleigh damping C_M in the model. In the damped region, the mechanical energy of the stress wave is viscously dissipated as energy in the material. It has been observed that high damping in the system results in increased resistance in the propagation of the stress wave in the damped layer and yield inaccurate readings.

Figure 3.2 represents the FE model showing a quarter section of the concrete plate with an ALID boundary region of length L_D. The length L_D is an important factor to consider while modeling ALID, as it affects the relative difference between the impedances of the elements in the wave absorbing region. A large difference in the impedance between the adjacent elements leads to internal reflections of the wave (Olsson, 2012).

35

3.7   WAVE PROPAGATION IN BOUNDED SOLIDS

The wave reflections from the side boundaries are important when studying stress wave propagation in bounded solids. Therefore to capture the boundary reflections, limitations are imposed on the locations where mechanical boundary conditions can be applied to support the model.

3.7.1   Foundation Layer Approach for Bounded Solids

A new approach for modeling wave propagation in bounded concrete sections is discussed. A flexible foundation layer having the same area as that of concrete plate of thickness T_f is used to support the concrete plate. The relative motion between the two parts is entirely eliminated by applying tie constraints.

The main concept behind the foundation layer approach is to create a reflecting interface at the base of the concrete plate such that the incident compression P-waves gets reflected back as tension waves (Refer Figure 3.3). This is made possible by defining a relatively low acoustic impedance for the foundation layer such that the coefficient of reflection R approaches -1. For the concrete/foundation layer interface of numerical model M3 (Refer Table 4.1) the value of R is calculated as **-0.94**. This indicates that most of the incident wave is reflected at the interface and there is phase change.

36

3.7.2 Modes of Vibration

Lin and Sansalone studied the transient response of rectangular (Lin & Sansalone, 1992) and circular bars (Lin & Sansalone, 1992) using IE method and identified resonant frequencies due to cross-sectional modes in the waveform. When the concrete foundation layer assembly is impacted by a load, various modes of vibrations including the thickness-mode are excited in the system.

The concrete plate supported by the foundation layer behaves as a rigid body supported on a soft spring with stiffness equal to the axial stiffness of the foundation layer. When this system is excited by an impact, the whole assembly vibrates in a piston-mode f_P similar to the compression and tension of a spring, and the frequency of this piston-mode can be detected in the amplitude spectrum.

3.7.2.1 Single Degree of Freedom Approximation

The dynamic characteristic of such systems can be approximated by using a single degree of freedom (SDOF) system represented Figure 3.4 (Chopra, 1995). In this study, the SDOF model comprised of a mass m_c, equal to that of a concrete slab, supported on a spring with stiffness equal to the axial stiffness of the foundation layer K_f given by Equation 3.7. Here, A is the area, E is the elastic modulus and T_f is the thickness of the foundation layer. The circular frequency ω_{SDOF} of the SDOF system is given by Equation 3.8 and the frequency in Hz is calculated by using Equation 3.9.

37

$$K_f = \frac{AE}{T_f} \qquad\qquad\qquad \textbf{3.7}$$

$$\omega_{SDOF} = \sqrt{\frac{K_f}{m_c}} \qquad\qquad\qquad \textbf{3.8}$$

$$f_{SDOF} = \frac{\omega_{SDOF}}{2\pi} \qquad\qquad\qquad \textbf{3.9}$$

3.7.2.2 Eigenvalue Analysis

The modes of vibration and corresponding natural frequencies of the concrete plate
supported on foundation layer can be obtained by performing an eigenvalue analysis.
Figure 3.5 shows the mode shape and frequency for four different modes (Mode 4, 9, 14
and 20) for concrete plate supported on (a) 100 mm and (b) 25 mm thick foundation
layer. When the assembly is impacted by the load, the resonant frequency (not the
thickness-mode f_T) corresponds to higher modes for models with a stiff foundation layer.

38
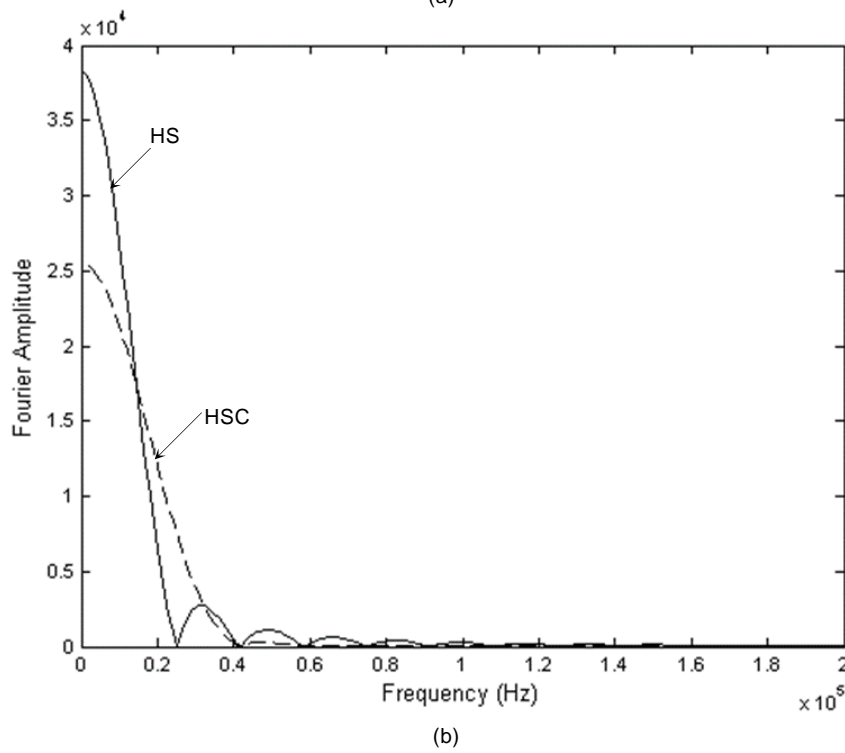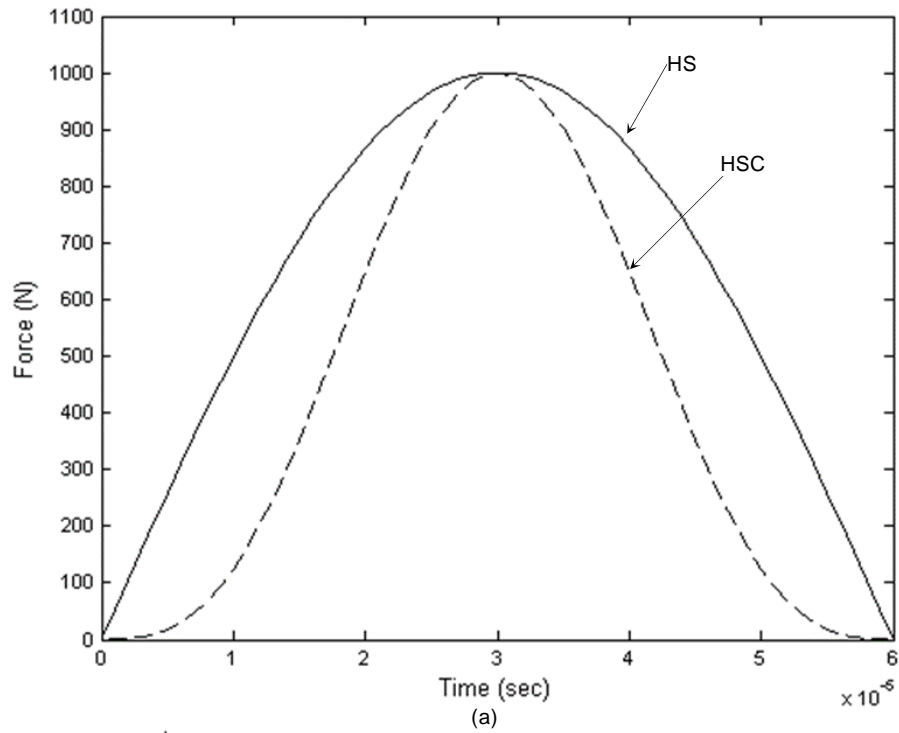
Figure 3.1   HS and HSC force-time function: (a) time history; and, (b) distribution of frequencies.

ALID
L_D

Concrete core

C3D8 w/o
damping

C3D8 with
damping
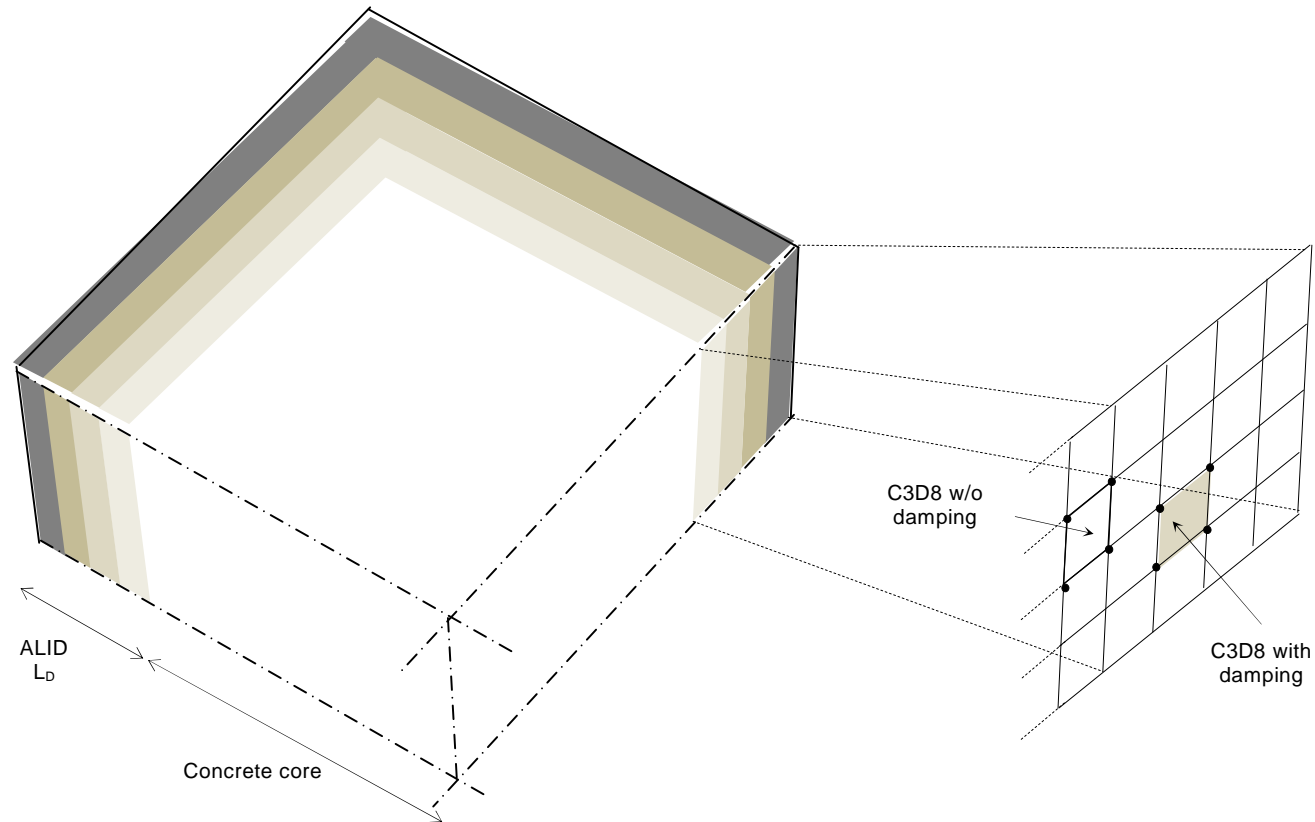
Figure 3.2   FE model showing a quarter section of the concrete plate with an ALID boundary region of length L_D as used in analysis M6.
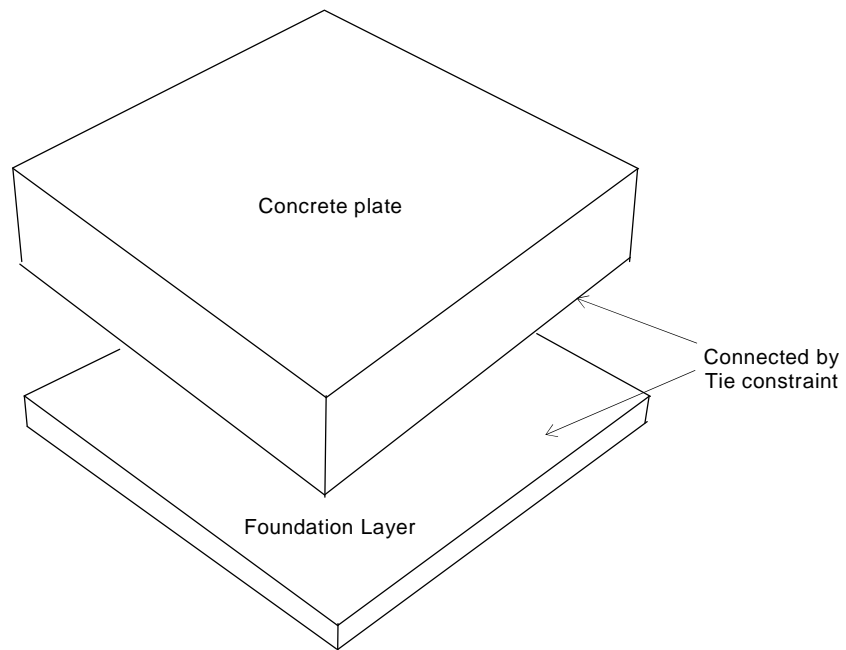
(a)
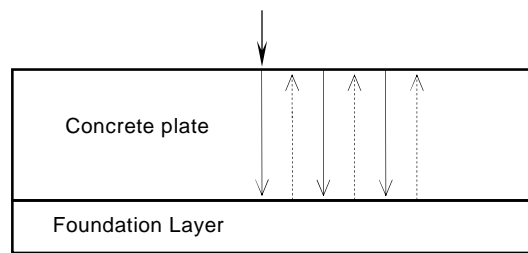
(b)

Figure 3.3   (a) Section showing concrete plate and foundation layer assembly, and (b) Stress wave behavior at the concrete/foundation layer interface.

41
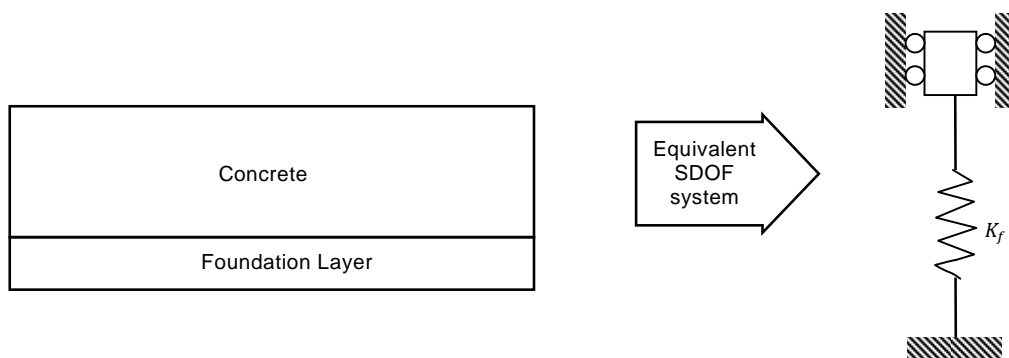
Figure 3.4   Representation of the FE model by an equivalent SDOF system.

	Mode 4	Mode 9	Mode 14	Mode 20
Freq. (Hz)	777	**1025**	1164	1255
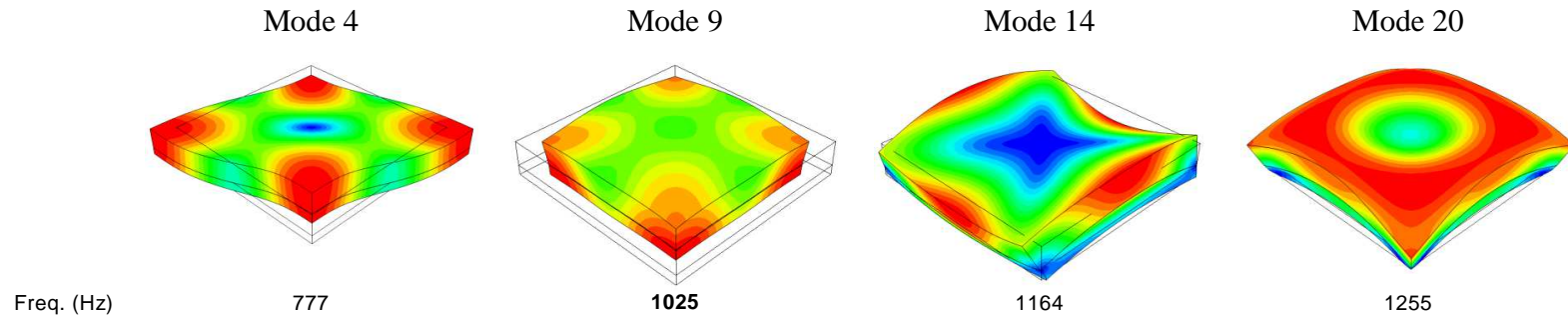
(a) Concrete plate supported on 100 mm thick foundation layer

Freq. (Hz)	770	1043	1616	**1949**
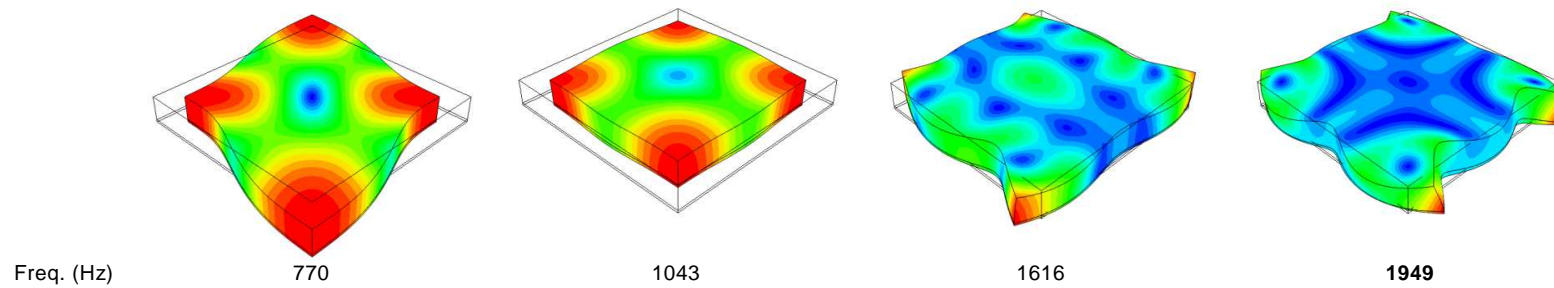
(b) Concrete plate supported on 25 mm thick foundation layer

Figure 3.5   Mode shapes and corresponding natural frequencies for concrete plate supported on foundation layer of thickness: (a) 100 mm, and (b) 25 mm.

43

CHAPTER 4. PARAMETRIC STUDY OF IMPACT ECHO MODELING PARAMETERS FOR CONCRETE SLAB EVALUATION

4.1 INTRODUCTION

This chapter describes the modeling approach for impact generated stress wave propagation in concrete plates. The numerical simulation of a concrete plate impacted by a steel sphere represented by force-time function was performed using FE software ABAQUS. Dynamic analyses for all the given cases were performed and time histories were recorded for a given time period. These waveforms in the time domain were then converted into frequency domain by the means of fast Fourier transform (FFT) to generate amplitude spectra for each case.

A list of parameters that influence the wave propagation characteristics was identified. A total of thirteen computer simulations for the propagation of impact generated stress waves were run by varying a particular parameter while keeping all the other constraints constant. The waveforms and the amplitude spectra thus obtained were examined to quantify the influence of each parameter in the wave propagation characteristics and thickness frequency detection accuracy. These parameters and their influence on the behavior of the propagated wave have been discussed in detail in the subsequent sections. The observations and result for each of the simulations are also discussed.

44

4.2   ANALYSIS MATRIX

Table 4.1 showcases an analyses matrix which tabulates the different parametric set analyzed in each simulation. These parameters were identified based on the in-depth literature review of the impact echo method and wave propagation theory in concrete and other medium. In the following subsections, each significant parameter is discussed in detail.

4.2.1   Impact Force-Time Function

The impact of a steel sphere on a concrete surface can be numerically represented by a force-time function as discussed in Section 2.2.1. The contact time t_c, the amplitude of the force F_{max} and the shape of the force-time function are the important properties that determine the frequency content of the pulse, and the magnitude of stresses and displacements of the particle motion.

For this study, two force-time formulations were considered; namely, half-cycle sine (HS) represented by Equation 2.8, and half-cycle sine cubed (HSC) given by Equation 2.9. Figure 4.1 represents the time history and frequency content of the two force formulations considered in this study.

A contact time t_c of 60 µs and maximum amplitude F_{max} of 1 kN was adopted to represent the drop of a 13 mm dia. steel sphere from a height of 0.3 m on the concrete plate.

45

$$t_c = 0.00858 \frac{r}{h^{0.1}} = 6.3 \times 10^{-5} s$$

$$F_{max} = \frac{1.140(v_o)^2 m_s}{\alpha_m} = 1.17 kN$$

$$v_o = \sqrt{2gh} = 1.98 m/s$$

$$\alpha_m = \left(\frac{15\pi v_o^2}{16(r)^{0.5}} (\delta_s + \delta_p) m_s \right)^{0.4} = 6.48 \times 10^{-5}$$

$$m_s = \rho_s \frac{4}{3} \pi r^3 = 9.03 \times 10^{-3} kg$$

$$\delta_s = \frac{1 - v_s^2}{\pi E_s} = 1.45 \times 10^{-12} m^2/N$$

$$\delta_p = \frac{1 - v_p^2}{\pi E_p} = 8.49 \times 10^{-12} m^2/N$$

4.2.2   Impact Force Distribution

The distribution of impact load on the concrete surface was identified as another important parameter that influenced the waveform characteristics. Two force distribution scenarios were used in the simulation as shown in Figure 4.2. In the first case, the HSC impact was applied as a point load over a single node at the impact location, and in the second case the HSC impact was imparted as a pressure load distributed over four elements at the impact location.

46

4.2.3 Impact Location

Three scenarios with locations I_1, I_2, and I_3 were studied to understand the effect of location of the impact load on the resultant waveform and spectrum. The position of these impacts on the concrete plate is shown in detail in Figure 4.3. Location I_1 represents the symmetric case in which the impact is imparted at the center of the plate and is thus farthest from the side boundary. This case was simulated to minimize the reflections from the sides and limit the excitation of higher flexural modes due to eccentricity in loading. Locations I_2 and I_3 are asymmetric loading cases, where the influence of the boundary reflections will distort the resulting waveform. The locations were chosen in a way that this influence would be higher for I_3 than I_2.

4.2.4 Mechanical Boundary Condition

In order to prevent rigid body motion, mechanical boundary conditions are required in FE software ABAQUS to perform transient dynamic analysis. Three different mechanical support/boundary conditions were investigated in this study which are discussed in the following subsections. These boundaries had dissimilar effects on the propagation of stress waves and the displacements waveforms which are subsequently discussed in detail in Section 5.3, 5.5 and 5.6.

4.2.4.1 Clamped Section

Clamped boundary condition utilizing pin supports were applied on the side of concrete section of size 2 m×2 m×0.25 m as shown in Figure 4.4. Applying pin supports at all boundary nodes restricts the translation and rotation of the plate in all directions.

4.2.4.2 Absorbing Layer with Increased Damping

An absorbing layer with increased damping (ALID) was studied to examine its effectiveness in absorbing the unwanted side reflections due to clamped boundary conditions. The energy absorbing ALID region of length L_D equal to 250 mm with specific values of mass proportional Rayleigh damping coefficient C_M, was built around an elastic concrete core as shown in Figure 4.5.

The energy absorbing region ALID, consisting of five different layers each measuring 50 mm in width (total length L_D of 250 mm), was built around the sides of the elastic concrete core. Each layer was assigned the same material properties as that of the concrete core with an additional mass proportional Rayleigh damping coefficient C_M. This coefficient introduces damping forces corresponding to the absolute velocities of the model and simulates a viscous damper that absorbs the boundary reflections. The value of C_M was chosen to increase in linear steps from 1000 to 19000 for each progressive layer.

48

4.2.4.3   Foundation Layer

The boundary condition for FE model of bounded section consisted of a flexible foundation layer on which the concrete plate was supported. The concrete and FL part were perfectly tied together to avoid relative deformation between them. Mechanical supports consisting of pin and roller supports as shown in Figure 4.6 were then applied at the bottom of the foundation layer to support the concrete-plate assembly. This restricted the vertical and horizontal translations, and rotations about the vertical axis of the concrete slab.

4.2.5   Foundation Layer Properties

The stiffness and the acoustic impedance of the foundation layer were identified as the major parameters that influence the waveform characteristics and effectiveness of the boundary condition in identifying the thickness frequency.

4.2.5.1   Stiffness

To evaluate the influence of foundation layer stiffness on the dynamic and wave propagation characteristics, a parameter R_K defined as ratio of plate stiffness to foundation layer stiffness was investigated. Four simulations with constant concrete plate stiffness and varying foundation layer stiffness were run. These values of the foundation layer stiffness were achieved by adopting a different foundation layer thickness while keeping the elastic modulus same.

49

4.2.5.2 Acoustic Impedance

To study the effect of acoustic impedance on the wave propagation and dynamic characteristics, a parameter R_Z defined as the ratio of acoustic impedance of plate to that of foundation layer was explored. As shown in Table 4.1, four simulations, each with a constant acoustic impedance of concrete plate and a different value of acoustic impedance of foundation layer were run. The specific value of impedance for foundation layer was achieved by varying the elastic modulus and density of the layer.

4.3   FINITE ELEMENT MODEL OVERVIEW

The finite element analysis of the propagation of impact generated stress wave in a concrete plate was carried out using FE software ABAQUS. Dynamic time history analysis was performed initially using the implicit solver in ABAQUS due to its unconditional stability. Simulations were also run using dynamic/explicit solver, which meet the conditional stability criteria discussed in Section 3.5.2. The use of an explicit solver yielded the same displacement histories as the implicit solver, but it significantly reduced overall computational time.

The force-time function was applied as an amplitude load at the impact location for each simulation. Displacement time-histories were recorded at nodes R_1, R_2, and R_3 at distance of 30 mm, 60 mm and 150 mm from the location of impact as shown in Figure 4.10. Each simulation was run for a total time of 1 ms and the displacements at the nodes were recorded at an interval of 1 µs. These time-histories were then processed using fast

50

Fourier transform (FFT) using Matlab to obtain the amplitude spectra in the frequency domain.

4.3.1 Section Properties

The concrete plate was modeled as a 3D deformable solid with dimensions measuring 2 m×2 m×0.25 m as shown in Figure 4.7 (a). An isotropic, homogenous and linear elastic material with properties listed in Table 4.2 was used to define the concrete medium. The P-, S- and R-wave velocities of the propagating stress wave in the concrete were calculated to be 4025 m/s, 2465 m/s and 2239 m/s respectively.

Similarly, the foundation layer with dimensions 2 m×2 m and variable thickness was modeled using an isotropic, homogenous and linear elastic material. The thickness of the layer was varied for different simulation cases as discussed in Section 5.5. The isometric view of a 25 mm thick foundation layer and its properties are given in Figure 4.7 (b) and Table 4.2 respectively.

4.3.2 Element Discretization

8-node linear brick continuum elements (C3D8) were used to discretize the concrete and the foundation layer in all the simulations. Figure 4.8 represents the FE model of the concrete and foundation layer sections. Elements of size of 10 mm×10 mm×10 mm were used as shown in Figure 4.9. A total of $1×10^6$ elements were used to represent the concrete plate (2 m×2 m×0.25 m) and 12,000 elements were used to represent the

51

foundation layer (2 m×2 m×0.025 m).The ALID boundary was also discretized in the

same manner as the concrete core with C3D8 linear elements of size

10 mm×10 mm×10 mm..

Table 4.1   Analysis matrix comparing various parameters used in the study.

ID	Force-time Function		Force Distribution		Impact Location			Boundary Condition			Foundation Layer Properties	
	HS	HSC	Point	Pressure	I_1	I_2	I_3	Clamped	ALID	Foundation Layer	R_K	R_Z
M1	✓		✓		✓					✓	1.16	34
M2		✓	✓		✓					✓	1.16	34
M3		✓		✓	✓					✓	1.16	34
M4		✓		✓	✓			✓				
M5		✓		✓	✓				✓			
M6		✓		✓	✓					✓	0.47	34
M7		✓		✓	✓					✓	2.33	34
M8		✓		✓	✓					✓	4.67	34
M9		✓		✓	✓					✓	1.16	5886
M10		✓		✓	✓					✓	1.16	111
M11		✓		✓	✓					✓	1.16	10.8
M12		✓		✓		✓				✓	1.16	34
M13		✓		✓			✓			✓	1.16	34

53

Table 4.2 **Properties of 250 mm thick structural concrete and 25 mm thick foundation layer.**

Property	Units	Concrete	Foundation Layer
Thickness, T	(mm)	250	25
Area	(m^2)	4	4
Modulus of elasticity, E	(GPa)	35	3
Poisson's ratio, ν	-	0.2	0.3
Density, ρ	(Kg/m^3)	2400	20
P-wave velocity, C_P	(m/s)	4025	14210
Acoustic impedance, Z	(Kg/m^2 $-$ s)	$9.66{\times}10^6$	$2.84{\times}10^5$
Axial stiffness, K	(N/m)	$5.6{\times}10^{11}$	$4.8{\times}10^{11}$

54
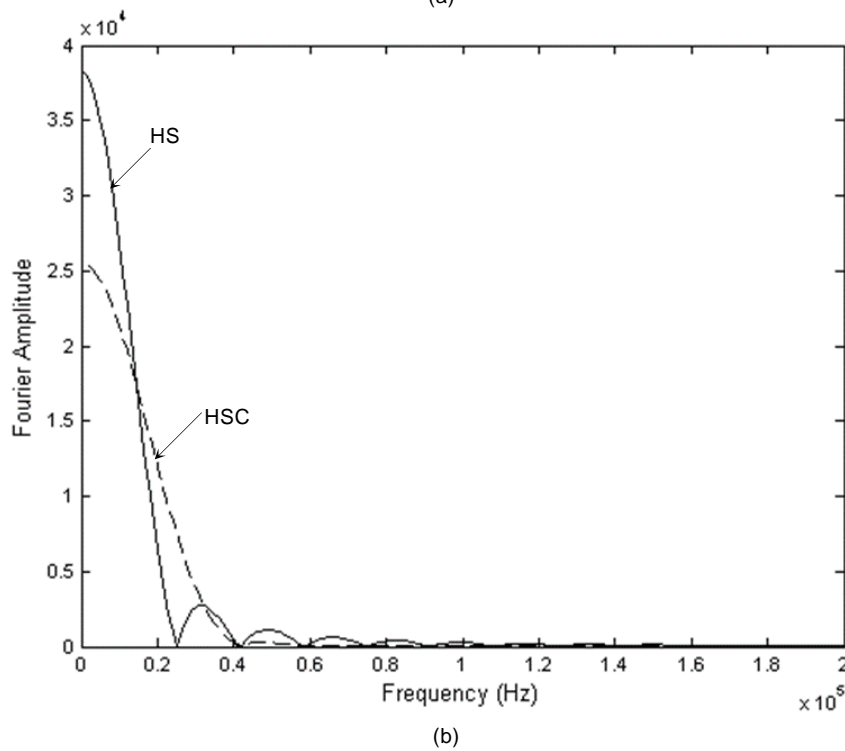
Figure 4.1   HS and HSC force-time function: (a) time history; and, (b) distribution of

frequencies.

55

(a)

All dimensions in mm

(b)
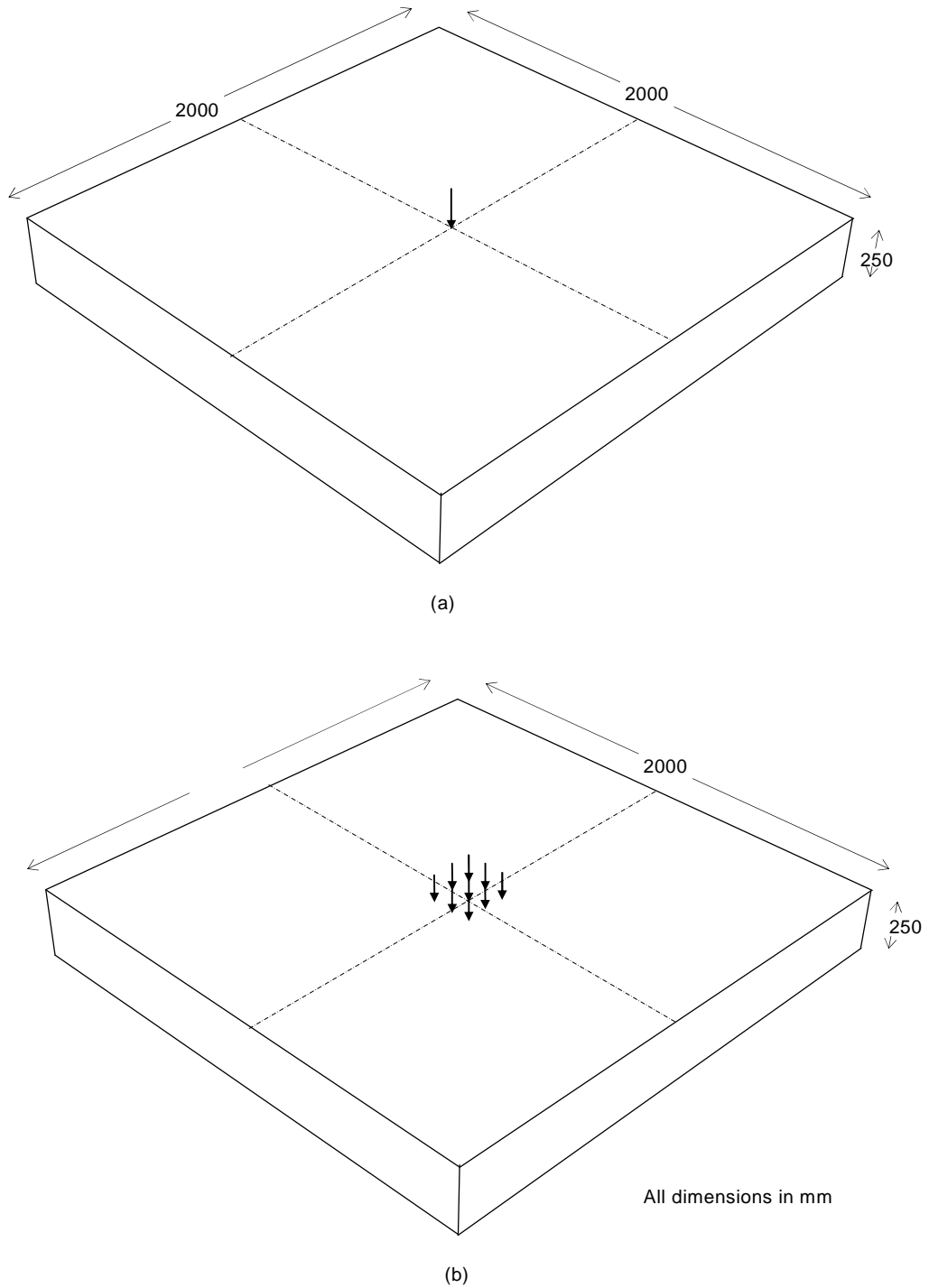
Figure 4.2   Distribution of impact force over: (a) single node; and, (b) nine nodes.

56
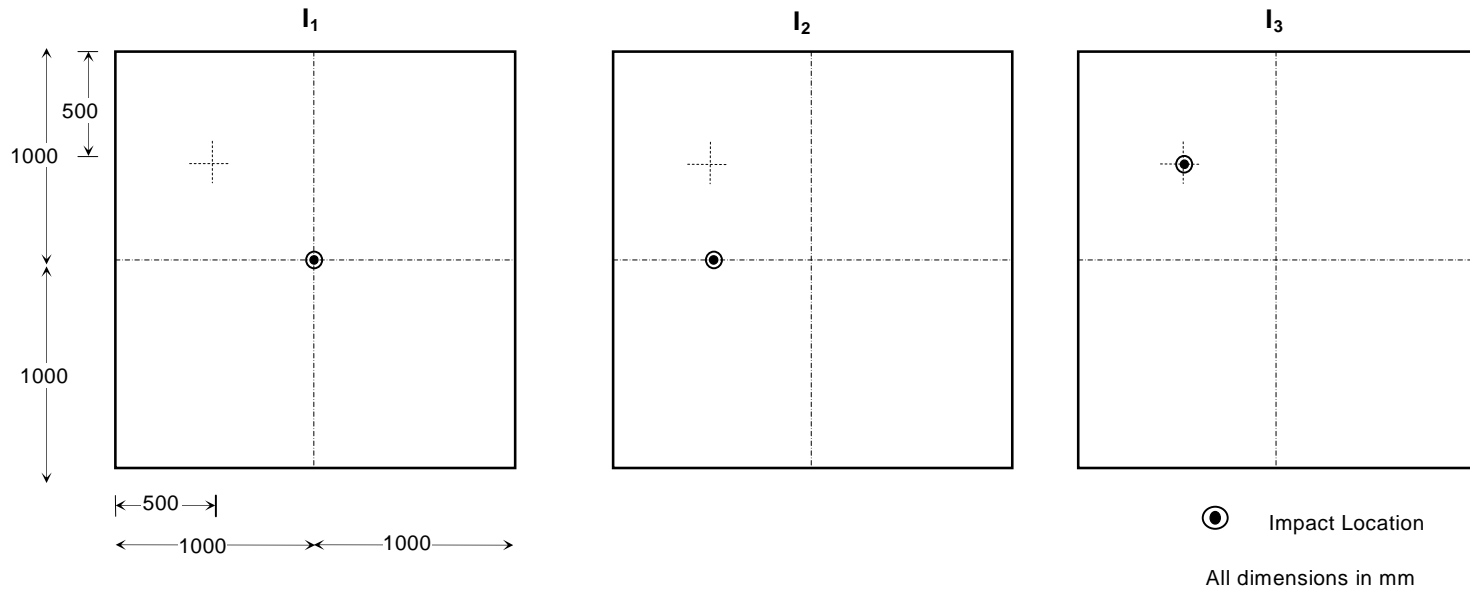
Figure 4.3   Plan showing locations of the impact load I₁, I₂, and I₃ on the concrete plate.
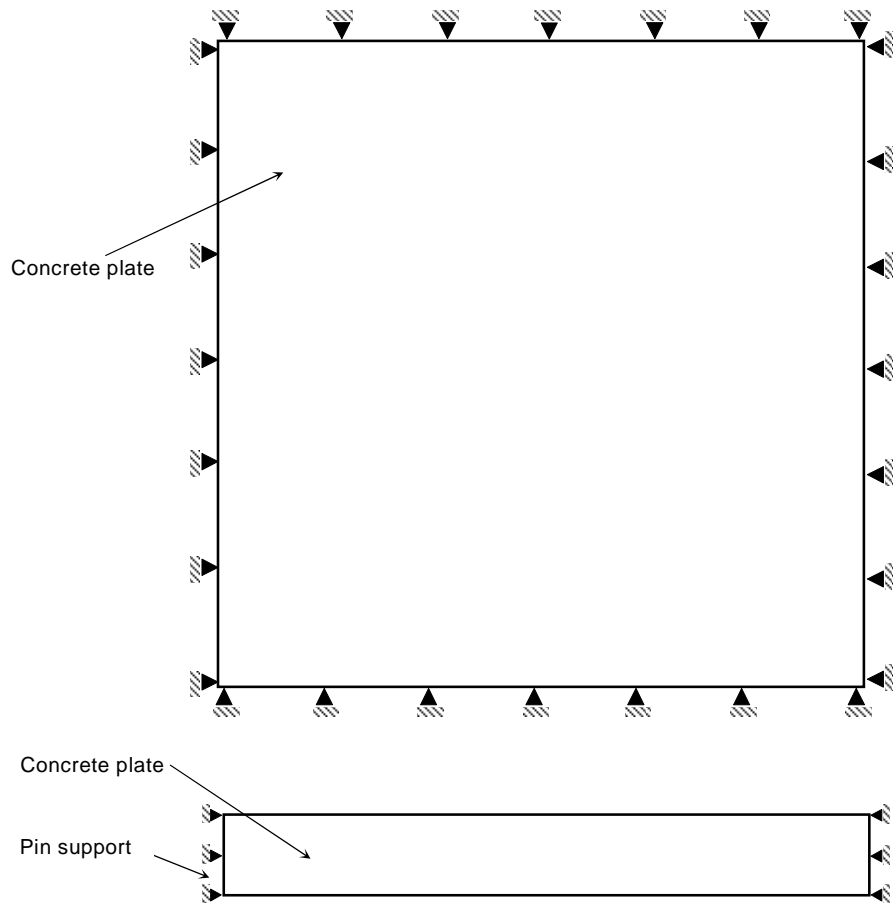
Figure 4.4   Clamped boundary support for concrete section pertaining to analysis M5.

58
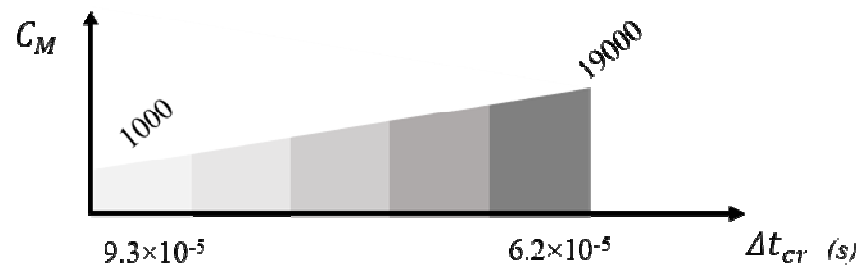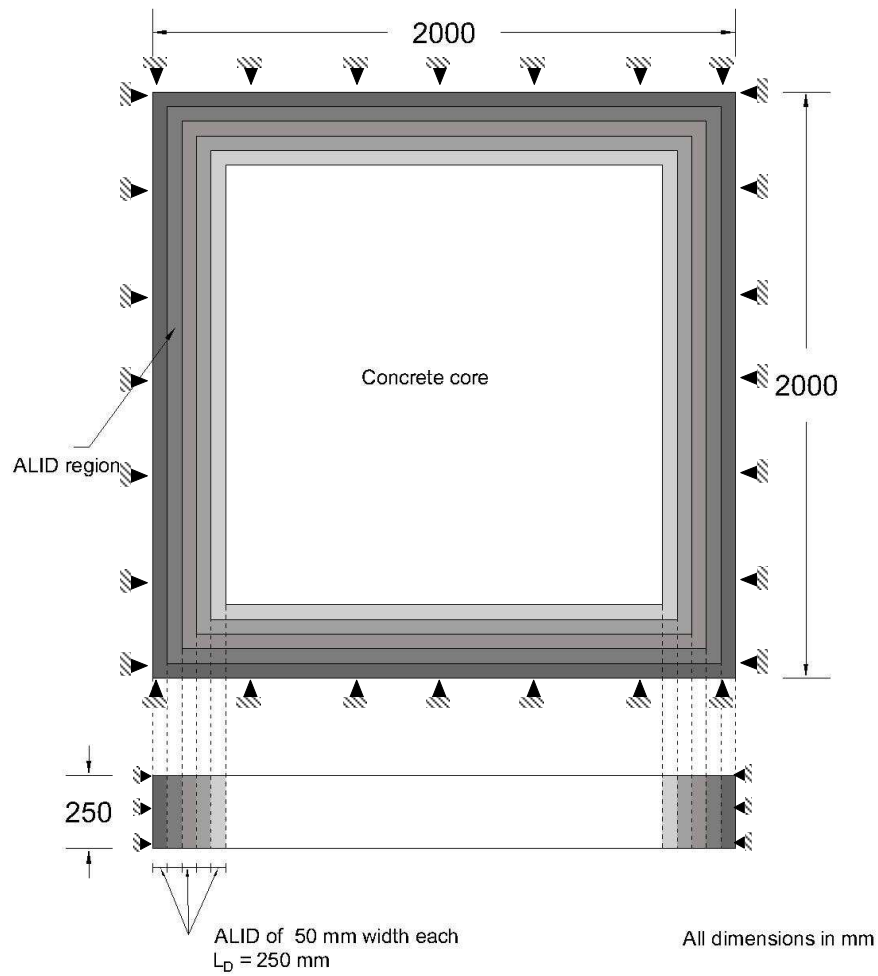
Figure 4.5   FE model showing a quarter section of the concrete plate with an ALID boundary region of length L$_D$ as used in analysis M6.

59
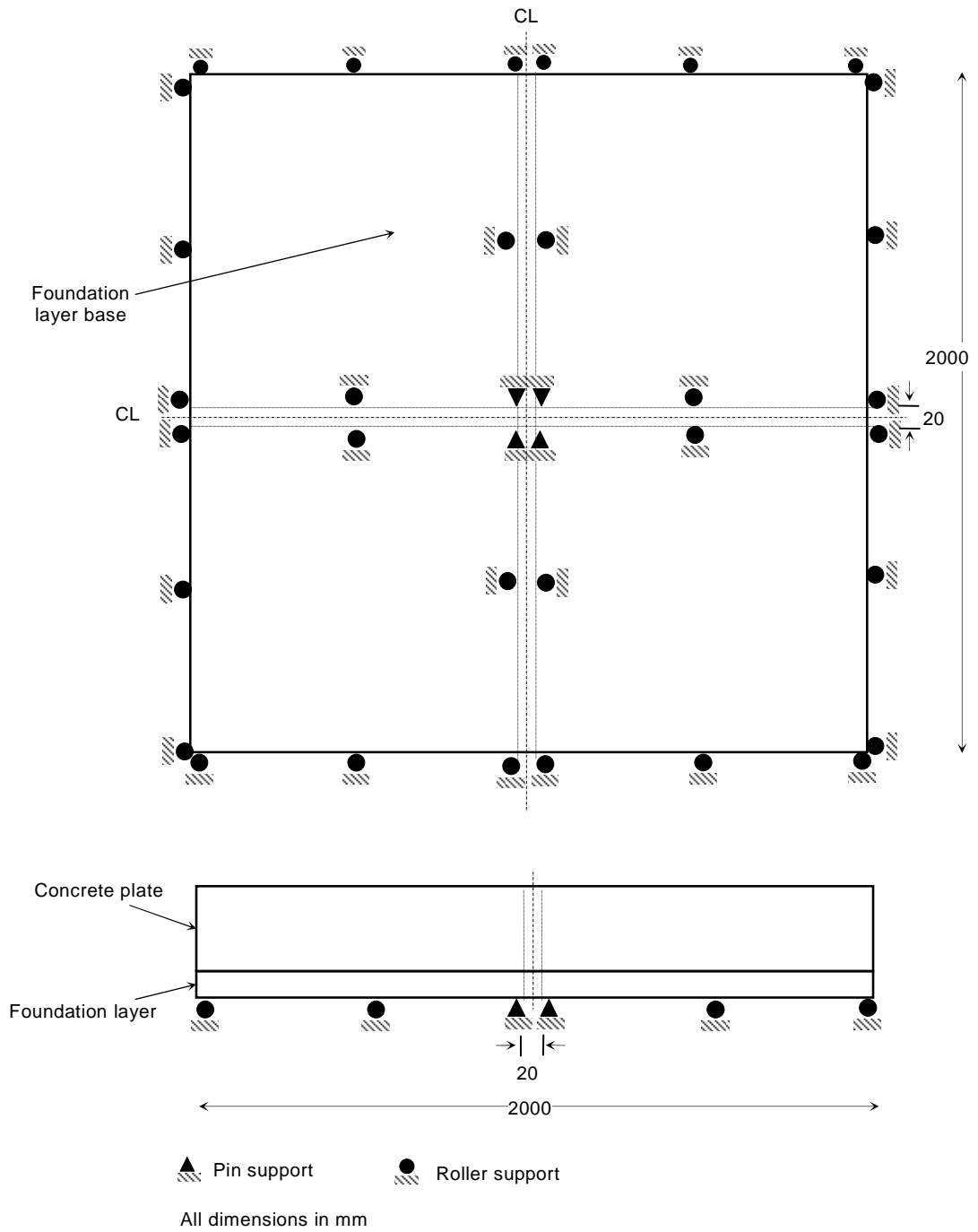
Figure 4.6   A typical arrangement of mechanical boundary support for FE models using a foundation layer.

60

2000

2000

250

(a)

2000

2000

25

All dimensions in mm

(b)
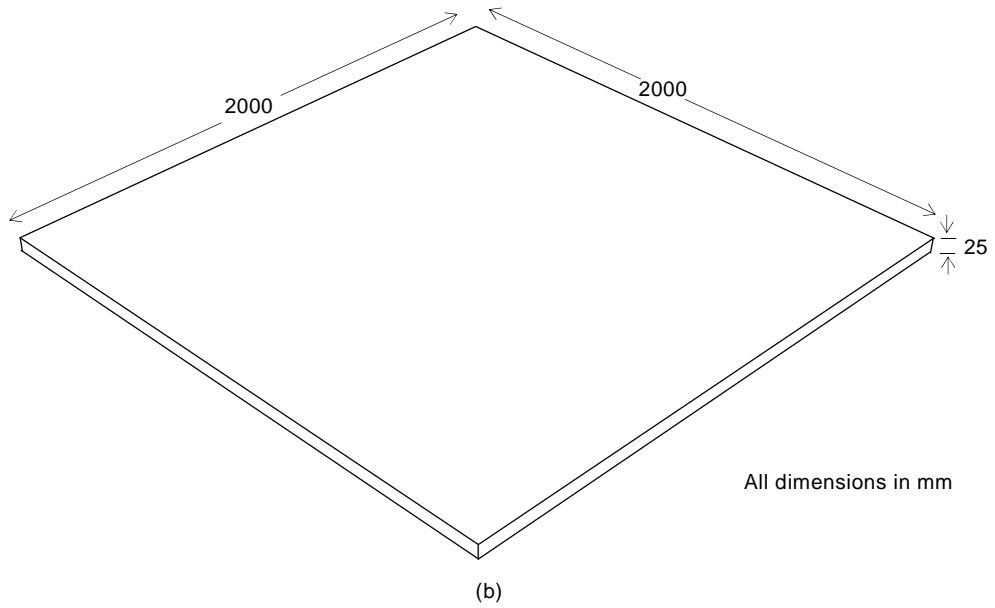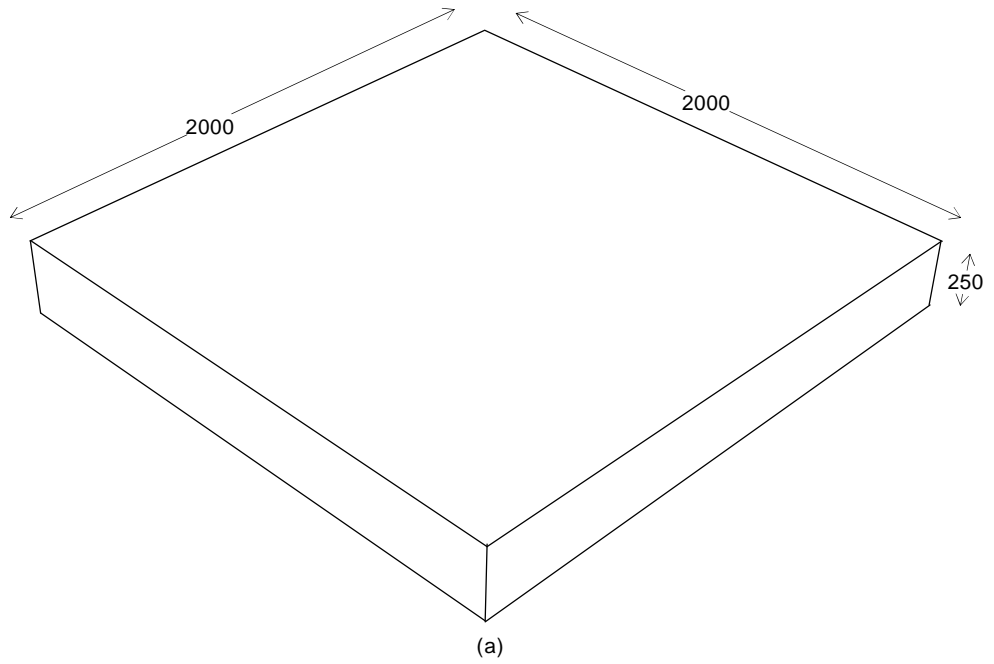
Figure 4.7   A typical section of: (a) concrete plate; and, (b) foundation layer.

61
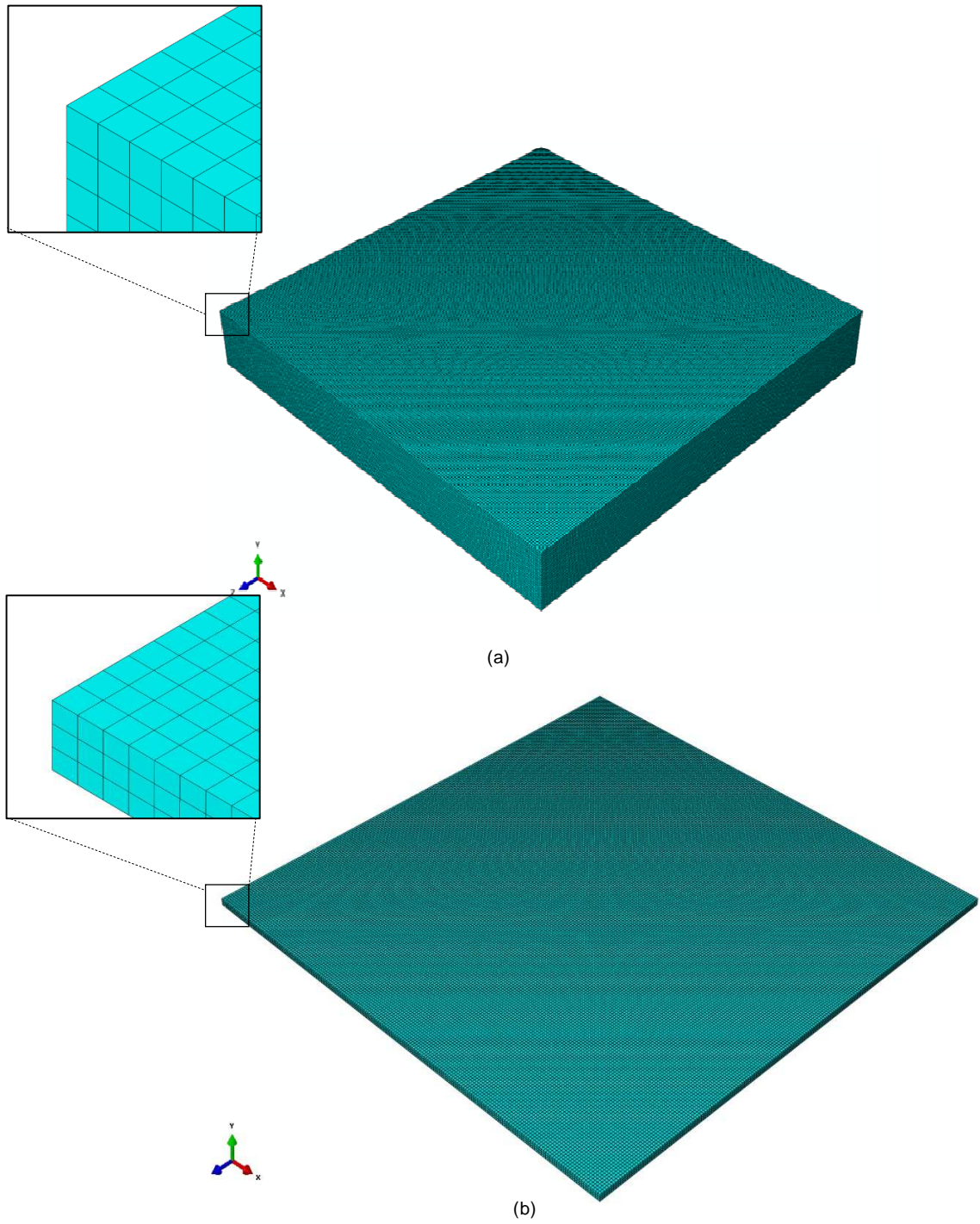
Figure 4.8   View of the FE model showing: (a) concrete part; and, (b) foundation layer part.

62
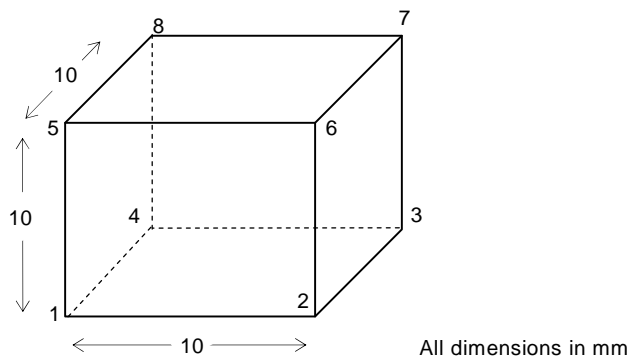
Figure 4.9   Overall size of C3D8 ABAQUS elements.

63
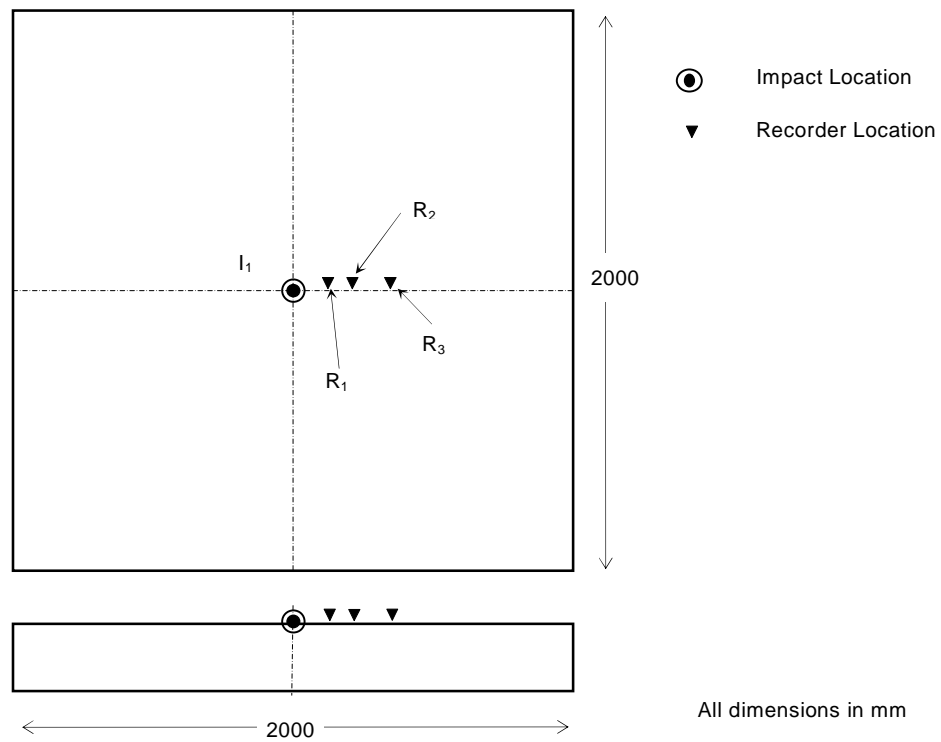
Figure 4.10 Plan (top) and elevation (bottom) showing typical location of recorders R_1, R_2, and R_3 at distances of 30 mm, 60 mm and 150 mm respectively from the point of impact I_1.

64

CHAPTER 5. RESULTS AND DISCUSSION

A total of thirteen FE simulations were run to study the influence of parameters identified in Chapter 4. In this chapter, the results and observations for the analysis cases are compared to signify the influence each parameter on wave propagation characteristics. Displacement time-histories recorded at node R_1 (at a distance 30 mm from impact location) was considered for comparing the waveforms for all the simulation. A frequency resolution of 122 Hz, achieved by zero-padding, was used to resolve the amplitude spectra in the frequency domain. The thickness-mode frequency f_T for the 0.25 m thick concrete plate was determined as 7671 Hz according to Equation 2.12.

5.1 IMPACT FORCE-TIME FUNCTION

Two simulations M1 with HS and M2 with HSC force-time functions (listed in Table 5.1) were run to study the effect of force-time function on the waveform characteristics. These force-time function parameters are introduced in Section 4.2.1.

Figure 5.1 compares the displacement time-histories for the two simulation cases. A high frequency artificial ringing was observed for M1, and this is attributed to the steeper initial slope of the HS force function. A gradual slope at the start of the applied force as in the case of HSC reduced the artificial ringing.

65

Figure 5.2 compares the amplitude spectra for the two cases. The artificial ringing observed for M1 in the displacement-time-history was also translated to the amplitude spectrum represented by the peak at 48 kHz. This ringing however does not hinder the accuracy of the amplitude spectrum in measuring the thickness-mode frequency. For both M1 and M2, the peak corresponding to the thickness-mode f_{th} was observed at 7813 Hz which is comparable to f_T of 7671 Hz. Another peak was observed at 1953 Hz which corresponds to the piston-mode frequency f_P of the system that is discussed in Section 3.7.2.

5.1.1 Summary

The formulation of force-time function is important in determining the maximum frequency of useful energy. For the same contact time t_c and amplitude F_{max} half-cycle sine cubed (HSC) yields a higher maximum useful frequency than the half-cycle sine (HS). Modeling the impact load by HS force-time function induces high frequency oscillations or "ringing" in the waveform. This can be eliminated by using HSC formulation which has a softer initial slope.

Table 5.1   Summary of analyses evaluated to study force-time function.

ID	Force-time Function		Force Distribution		Impact Location			Boundary Condition			Foundation Layer Properties	
	HS	HSC	Point	Pressure	I_1	I_2	I_3	Clamped	ALID	Foundation Layer	R_K	R_Z
M1	✓		✓		✓					✓	1.16	34
M2		✓	✓		✓					✓	1.16	34

Figure 5.1   Comparison of displacement time-history for models with force-time function modeled as HS (M1) and HSC (M2).
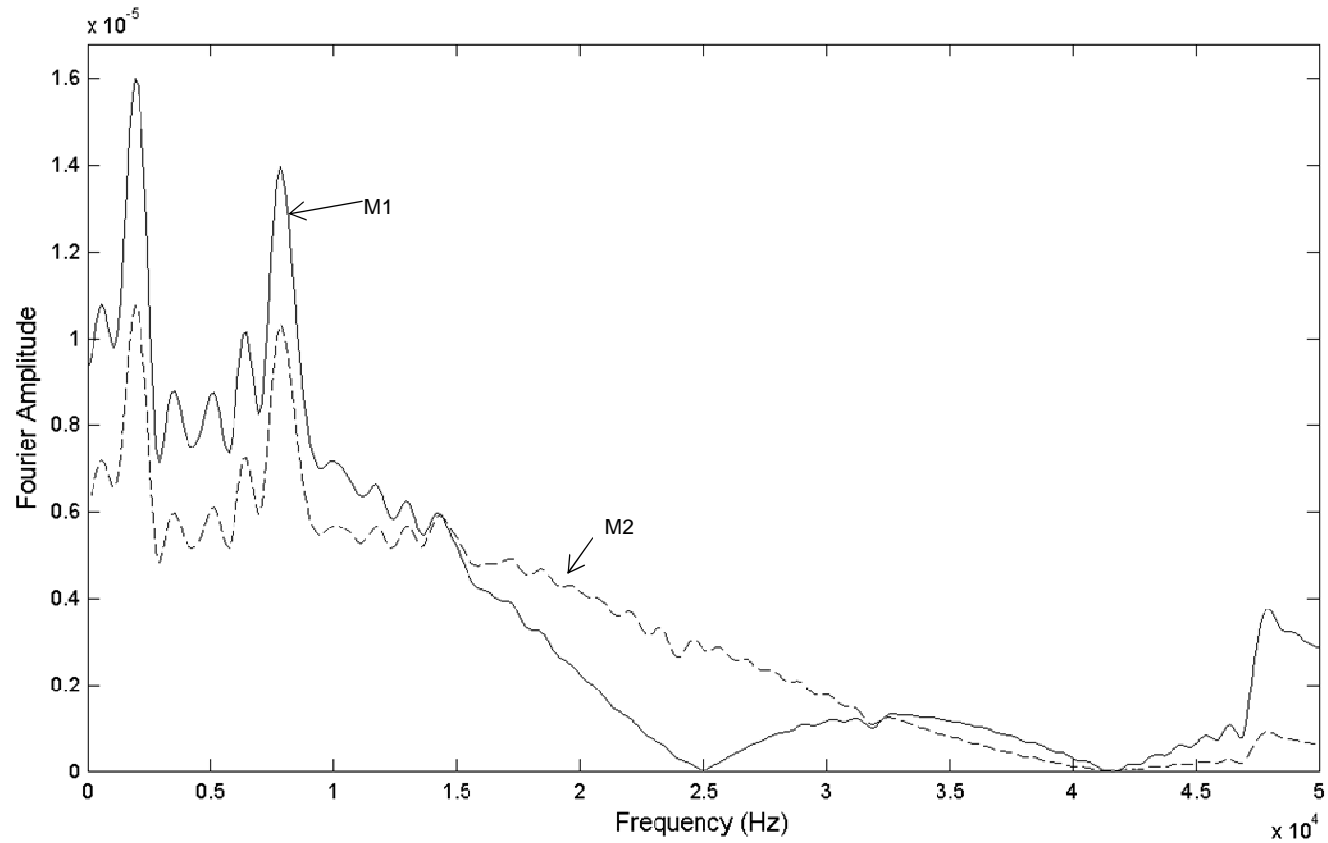
Figure 5.2   Comparison of amplitude spectra for models with force-time function modeled as HS (M1) and HSC (M2).

5.2 IMPACT FORCE DISTRIBUTION

Two simulations were run with HSC force-time loading distributed over; (a) single node for M2; and, (b) nine nodes (four elements) for M3 (Refer Table 5.2). Figure 5.3 represents the time-histories for the two cases.

In the case of M2, applying the impact over a single node led to localized deformations on the surface and undulations were observed at the beginning of the displacement time-history. Redistributing the impact load over four elements helped in eliminating the undulations due to localized deformations.

Figure 5.4 shows the amplitude spectra for models M2 and M3. No notable difference except in the amplitude values were observed for both the case. The piston-mode and thickness-mode frequency peaks were observed at 1953 Hz and 7813 Hz for both the cases.

5.2.1 Summary

Localized deformation of the concrete surface takes place (represented by undulations in the displacement history) when the impact load is concentrated over a single node. This effect can be eliminated by modeling the impact load as a pressure load distributed over two or more nodes. However modeling the impact as concentrated load does not affect the accuracy of the thickness-mode frequency.

70

Table 5.2   Summary of analyses evaluated to study force distribution parameter.

ID	Force-time Function		Force Distribution		Impact Location			Boundary Condition			Foundation Layer Properties	
	HS	HSC	Point	Pressure	I_1	I_2	I_3	Clamped	ALID	Foundation Layer	R_K	R_Z
M2		✓	✓		✓					✓	1.16	34
M3		✓		✓	✓					✓	1.16	34
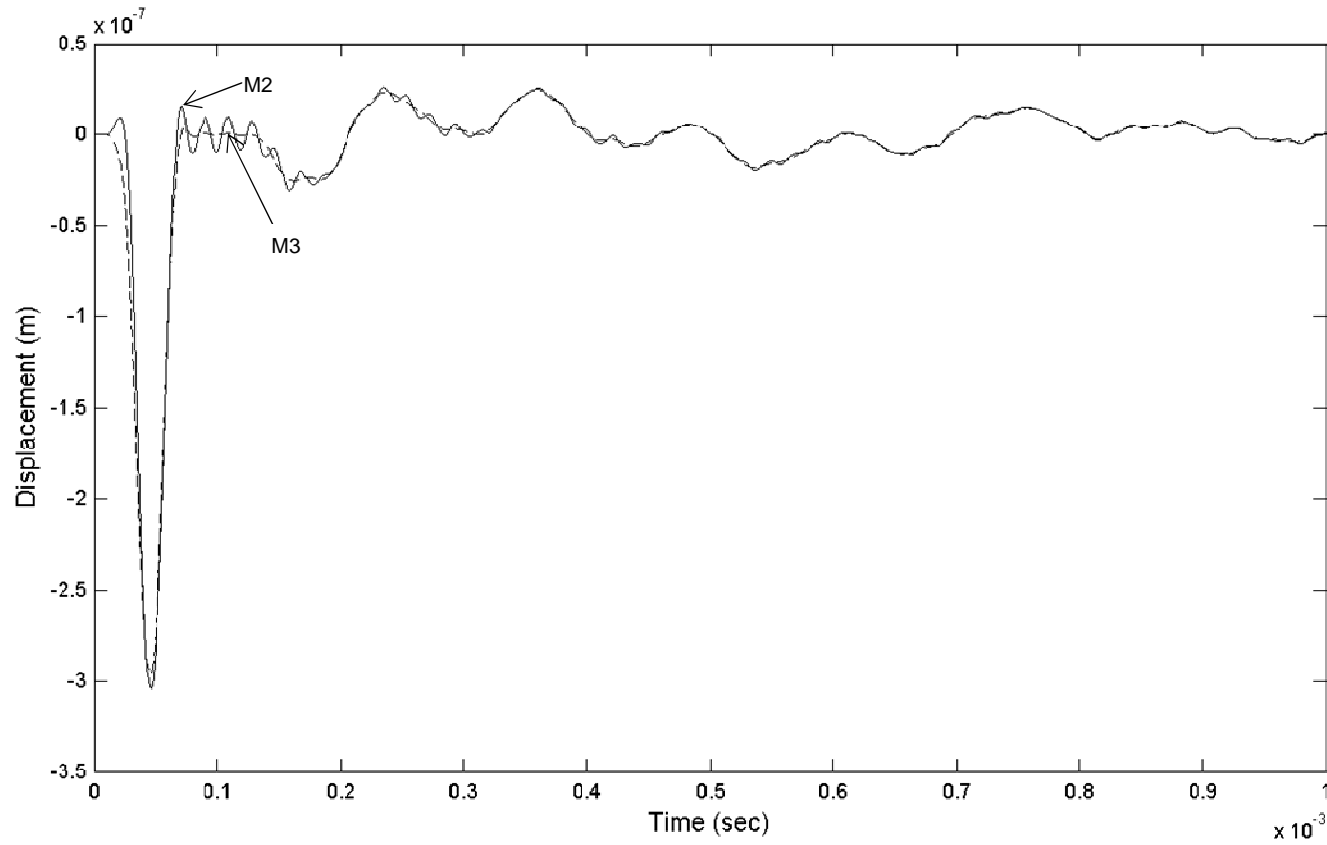
Figure 5.3   Comparison of displacement time-history for models with impact load distributed over single node (M2) and multiple node (M3).
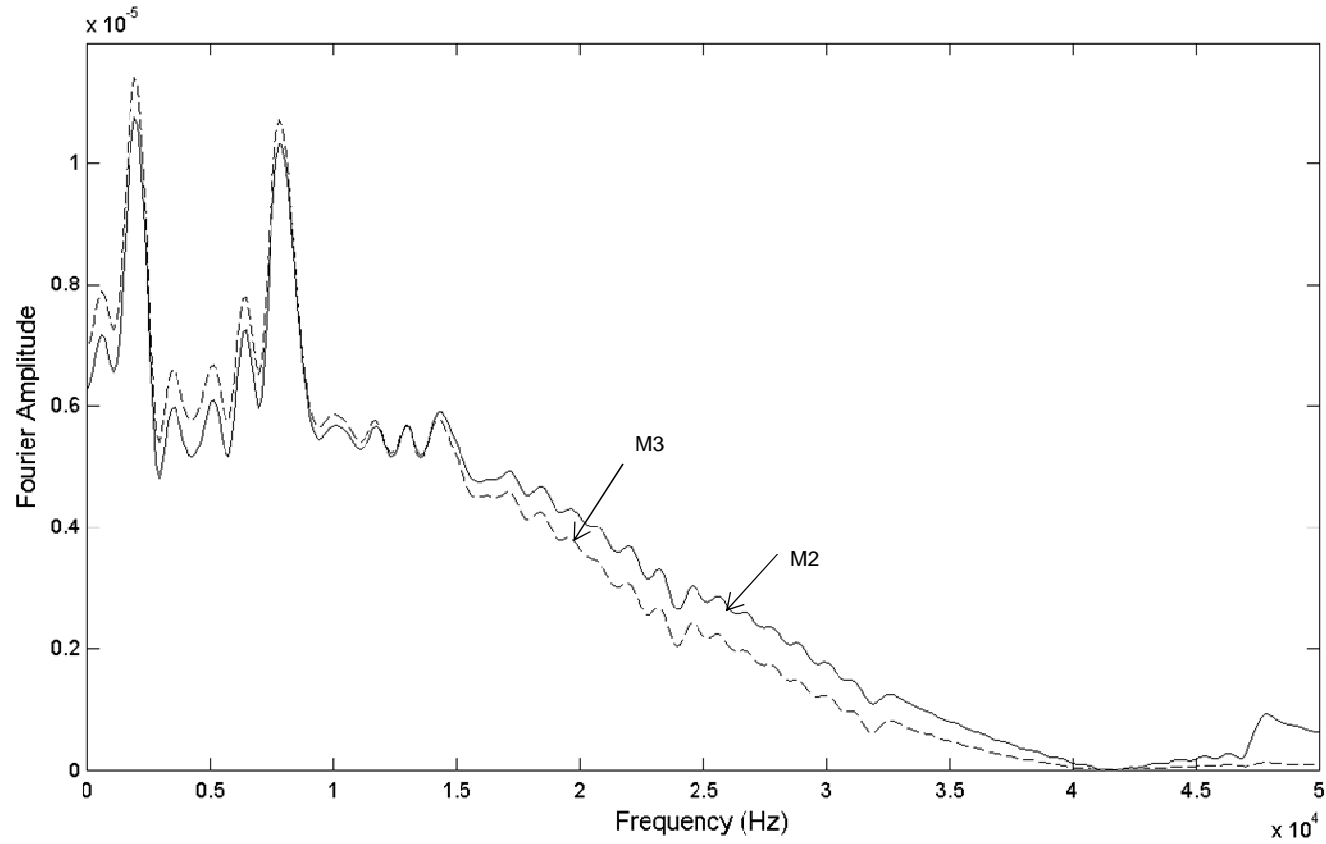
Figure 5.4   Comparison of amplitude spectra for models with impact load distributed over single node (M2) and multiple node (M3).

5.3   IMPACT LOCATION

Three simulations, M3, M12 and M13, given in Table 5.3 were run to study the influence of location of impact load imparted at sites I_1, I_2, and I_3 as discussed in Section 4.2.3. The HSC force-time function distributed over four elements was used at the impact site for all the three simulations. The concrete plate was supported by a foundation layer and mechanical boundary condition defined in Section 4.2.4.3 was considered.

Figure 5.5 compares the displacement time-histories for the three models and it was observed that the displacements for I_2, and I_3 (eccentric load cases) differ from that for I_1 (symmetric load case) starting at 5P. This difference becomes more pronounced at 10P when higher amplitudes and frequencies in the displacement history were observed. This behavior is attributed to the reflected waves reaching the recorder location earlier for I_2 and I_3 locations as compared for I_1 location.

Figure 5.6 compares the amplitude spectrum for the three models. For all the three models, thickness-mode and piston-mode frequencies were identified at 7813 Hz and 1953 Hz respectively. For models M12 and M13, the effect of higher frequency wave reflections was observed which may present difficulty in detecting the thickness-mode frequency.

74

5.3.1 Summary

For the concrete plate with foundation layer boundary condition, eccentric impact loading does not excite any higher flexural mode other than the piston-mode of the foundation layer. However, the displacement histories for eccentric deviates from that of symmetric loading at around 5P owing to the early arrival of the P-waves reflected from the free boundary of the concrete plate. This deviation becomes profound at around 10P during which the side wave reflections increases.

75

Table 5.3   Summary of analyses evaluated to study influence of impact load location.

ID	Force-time Function		Force Distribution		Impact Location			Boundary Condition			Foundation Layer Properties	
	HS	HSC	Point	Pressure	I_1	I_2	I_3	Clamped	ALID	Foundation Layer	R_K	R_Z
M3		✓		✓	✓					✓	1.16	34
M12		✓		✓		✓				✓	1.16	34
M13		✓		✓			✓			✓	1.16	34
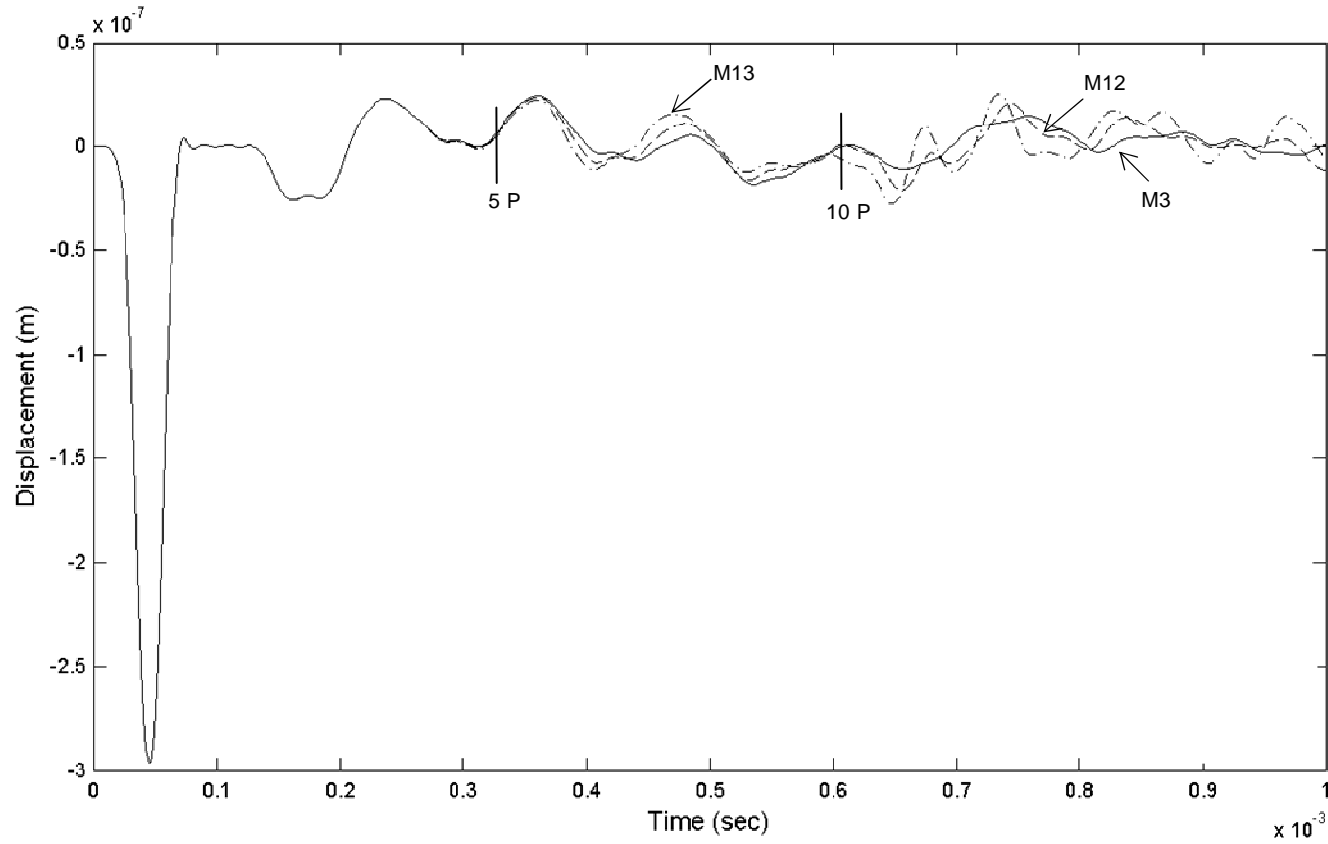
Figure 5.5   Comparison of displacement time-histories for different impact locations on a concrete plate.
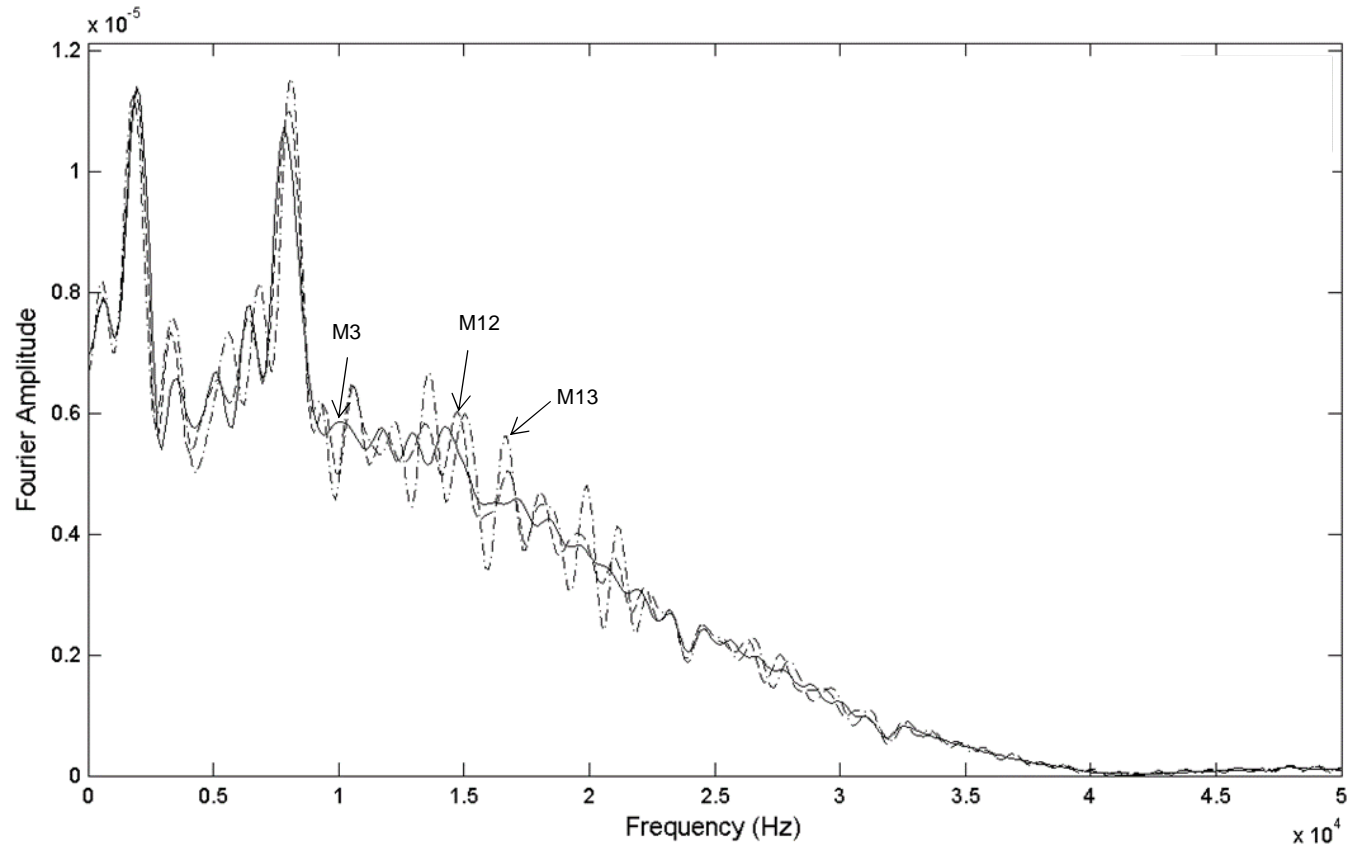
Figure 5.6   Comparison of amplitude spectra for different impact locations on a concrete plate.

5.4 BOUNDARY CONDITION

To study the effect of the boundary condition on the propagating stress waves, three simulations M4, M5 and M8 were run (Table 5.4). Model M4 consisted of a concrete plate of 2m ×2 m ×0.25 m dimensions supported by a clamped boundary. Model M5 consisted of an ALID region built around the sides of the elastic concrete plate (with dimensions, 1.5 m ×1.5 m ×0.25 m). The ALID (L_D of 250 mm) region comprised of five subsequent layers, each measuring 50 mm in width and having a specific value of C_M. Model M8 consisted of a 2m ×2 m ×0.25 m concrete plate supported on a 2m×2 m×0.1 m foundation layer with material properties listed in Table 4.2.

Figure 5.7 represents the displacement time-histories for three models. It was observed that the influence of the boundary reflections in M4 disrupts the waveform pattern as the arrival of P-waves was no easily distinguishable. Adding the wave attenuating region (ALID) absorbed these side reflections and produced a more uniform waveform. The displacement waveform for the foundation layer (M8) is quite similar to that of M5 (ALID) and the arrival P-waves are easily distinguishable.

Figure 5.8 shows the amplitude spectrum for the three analysis cases. The peak for M4 was observed at 3662 Hz which was very different from the calculated thickness-mode frequency f_T of 7671 Hz. For case M5, a peak was observed at 7568 Hz which was very close to the estimated f_T frequency. For M8, two distinct peaks were observed at 7690 Hz and 1465 Hz which corresponds to the thickness-mode, f_{th} and piston-mode, f_P frequencies respectively.

79

5.4.1 **S**ummary

For a semi-infinite section, wave reflections from the clamped boundaries influence the displacement time-history and yield erroneous peak frequency in the amplitude spectrum. To avoid such discrepancies a sufficiently large model can be built to shun the effect of boundary reflections for the analysis time. This however adds extensively to the computational cost. The same effect can also be achieved by using non-reflecting or absorbing boundaries.

A significant reduction in model's geometric size and computational cost can be achieved by implementing the absorbing layer with increased damping (ALID) boundary condition. While modeling the ALID boundaries, the length L_D and the mass proportion Rayleigh damping coefficient C_M affects it efficiency in attenuating the amplitude of the propagating wave.

The foundation layer approach was successfully applied to study the wave propagation in concrete plates of a finite dimension. The amplitude spectrum of the system consisting of a concrete plate supported on flexible foundation layer is dominated by the piston-mode and thickness-mode frequencies.

Table 5.4   Summary of analyses evaluated to study the effect of boundary condition.

ID	Force-time Function		Force Distribution		Impact Location			Boundary Condition			Foundation Layer Properties	
	HS	HSC	Point	Pressure	I_1	I_2	I_3	Clamped	ALID	Foundation Layer	R_K	R_Z
M4		✓		✓	✓			✓				
M5		✓		✓	✓				✓			
M8		✓		✓	✓					✓	4.67	34
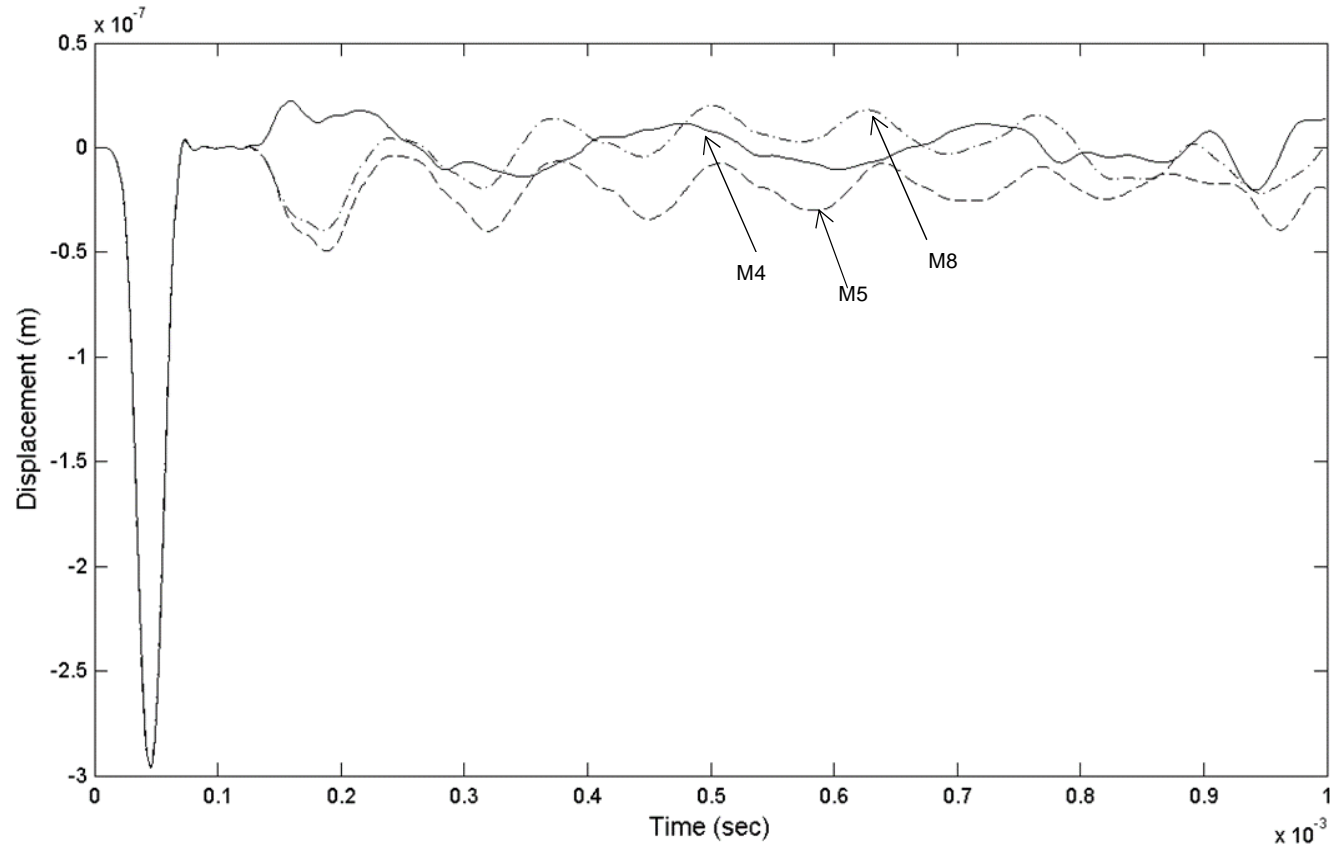
Figure 5.7   Comparison of displacement time-histories for models with clamped boundary (M4) and ALID (M5).
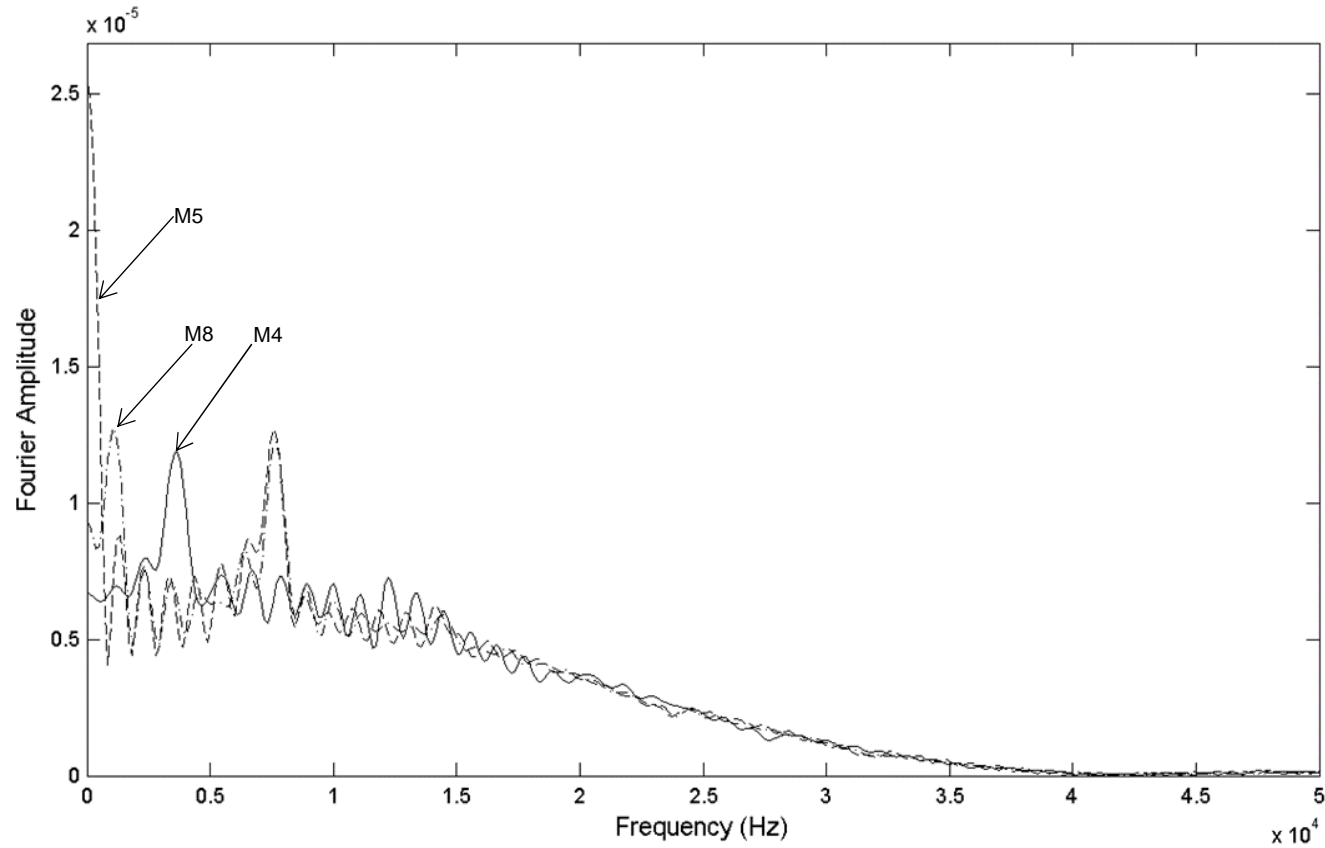
Figure 5.8   Comparison of amplitude spectra for models with clamped boundary (M4) and ALID (M5).

5.5 PLATE-FOUNDATION LAYER STIFFNESS RATIO R_K

Four simulations M3, M6, M7 and M8 with concrete plate-foundation stiffness ratio R_K of 1.16, 0.47, 2.33 and 4.67 were analyzed as summarized in Table 5.5. These values of stiffness ratio were obtained by varying the thickness of the foundation layer for each model (as given in Table 5.5) while keeping all other properties of the foundation layer constant. No change to the section or material properties of the concrete plate was made.

Figure 5.9 represents the displacement time-histories for the set of simulations used in this parametric study. The amplitude and period of the displacements varied for the different simulations. The amplitude spectra for the respective models are shown in Figure 5.10. The piston-mode frequencies were also detected in the FFT plot, and their values are listed in Table 5.6 along with thickness-mode frequencies. The fundamental frequencies of the equivalent SDOF system are also presented in this table.

The FFT plot for analysis case M6 with R_K value of 0.47 showed some ambiguity in the detection of thickness-mode frequency represented by two closely spaced peaks at 7935 and 8789 Hz. For all other analysis cases, distinct peaks were identified as the thickness-mode frequency.

Figure 5.11 shows the vibration mode excited for model M3 and M8. For model M8 (flexible foundation layer) Mode 9 was excited. For model M3 (stiff foundation layer) a higher mode, i.e. Mode 20, was excited by the impact load.

84

5.5.1 Summary

The ratio of the plate stiffness to the foundation layer stiffness R_K determines the piston-mode frequency of concrete-foundation layer assembly. A higher value of R_K, that represents a more flexible foundation layer, improves the accuracy of the amplitude spectrum in distinguishing the thickness-mode and piston-mode frequency. A stiffer foundation layer possess ambiguity in distinguishing the thickness-mode frequency from the amplitude spectrum.

Concrete plate supported on flexible foundation layer behaves as a rigid mass supported on soft spring and vibrates in piston-mode that is easily detected in the amplitude spectrum as a distinct peak. This mode of vibration can also be estimated by calculating the fundamental frequency of a SDOF model comprising rigid mass (equal to mass of concrete plate) supported on a spring of stiffness K_f (axial stiffness of foundation layer).

Table 5.5   Summary of analyses evaluated to study the effect stiffness ratio.

ID	Force-time Function		Force Distribution		Impact Location			Boundary Condition			Foundation Layer Properties	
	HS	HSC	Point	Pressure	I_1	I_2	I_3	Clamped	ALID	Foundation Layer	R_K	R_Z
M3		✓		✓	✓					✓	1.16	34
M6		✓		✓	✓					✓	0.47	34
M7		✓		✓	✓					✓	2.33	34
M8		✓		✓	✓					✓	4.67	34

Table 5.6   Table summarizing FE models with varying axial stiffness property of foundation layer.

ID	Foundation Layer			R_K	Frequency			
	T	E	K_f		f_{th}	f_T	f_P	f_{SDOF}
	(mm)	(GPa)	(N/m)		Hz	Hz	Hz	Hz
M6	10	3	1.2×10^{12}	0.47	8789	7671	2563	3561
M3	25	3	4.8×10^{11}	1.16	7813	7671	1953	2252
M7	50	3	2.4×10^{11}	2.33	7690	7671	1465	1592
M8	100	3	1.2×10^{11}	4.67	7690	7671	1009	1126

Note: the area of the foundation layer is 4 m^2 for all cases
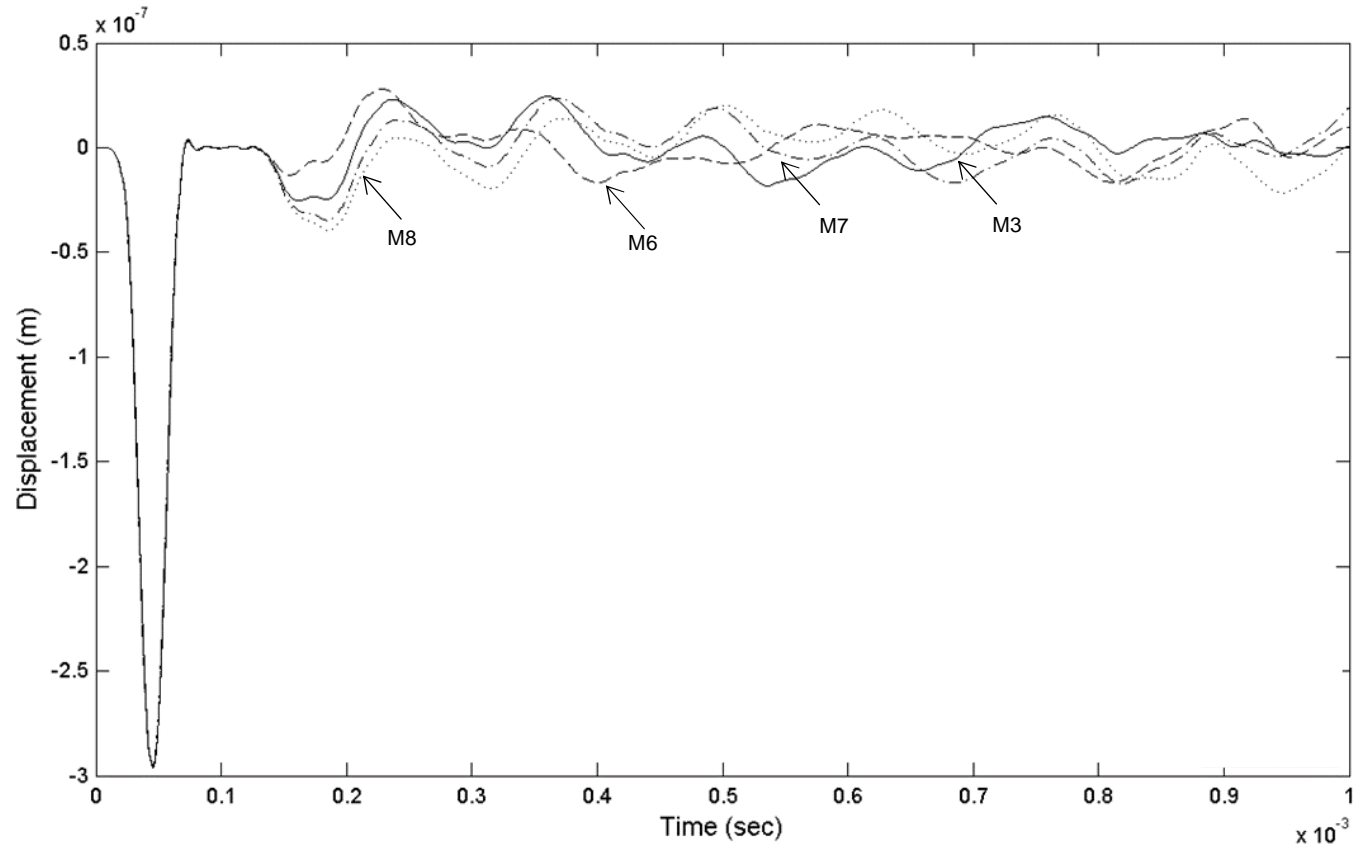
Figure 5.9   Comparison of displacement time-histories for the models with varying thickness of foundation layer.
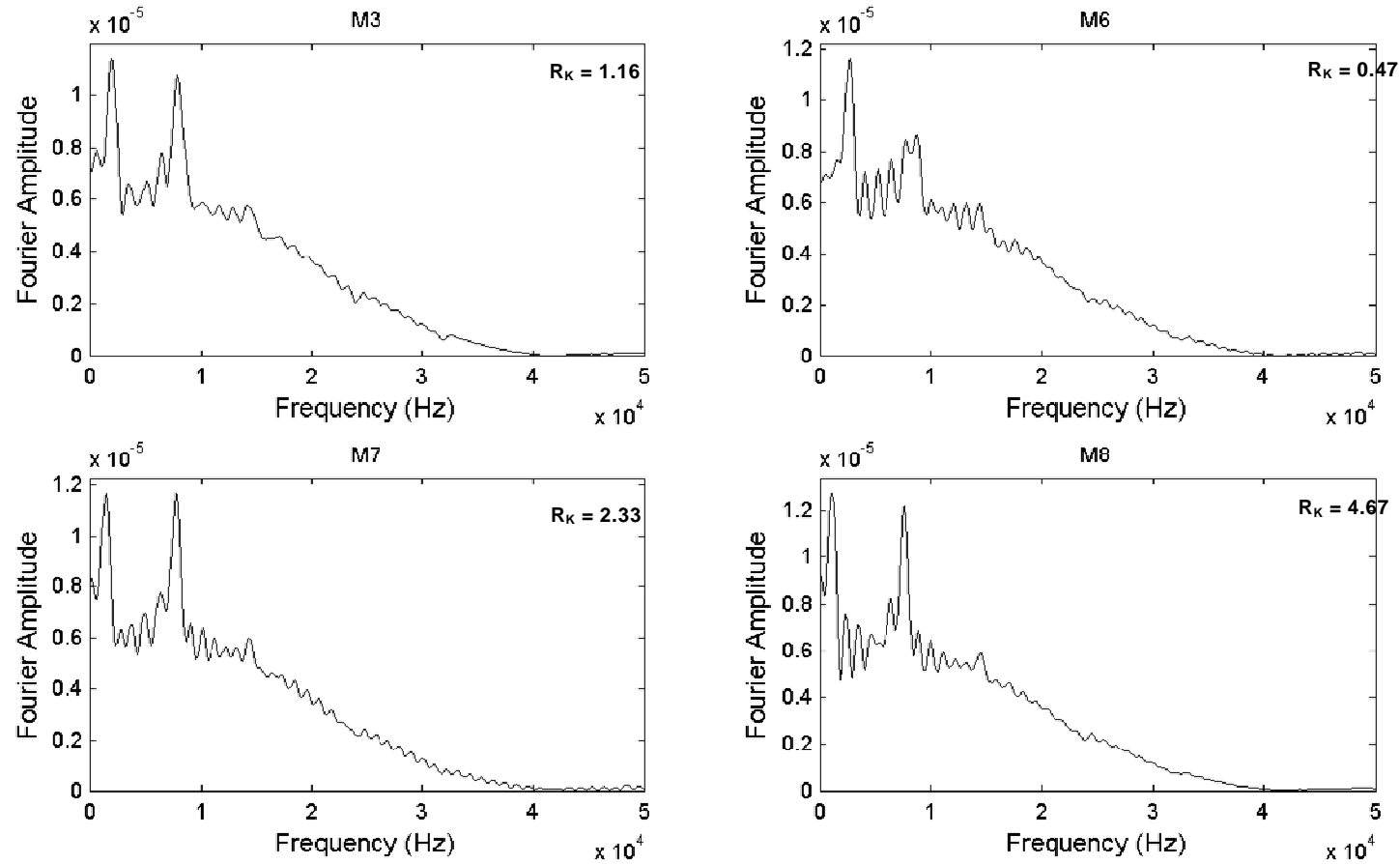
Figure 5.10   Comparison of amplitude spectra for the models with varying thickness of foundation layer.

U, Magnitude
+1.379e+00
+1.307e+00
+1.234e+00
+1.161e+00
+1.089e+00
+1.016e+00
+9.437e-01
+8.711e-01
+7.985e-01
+7.259e-01
+6.533e-01
+5.807e-01
+5.081e-01
+4.356e-01
+3.630e-01
+2.904e-01
+2.178e-01
+1.452e-01
+7.259e-02
+0.000e+00

(a)

Mode 20, 1949 Hz

(b)
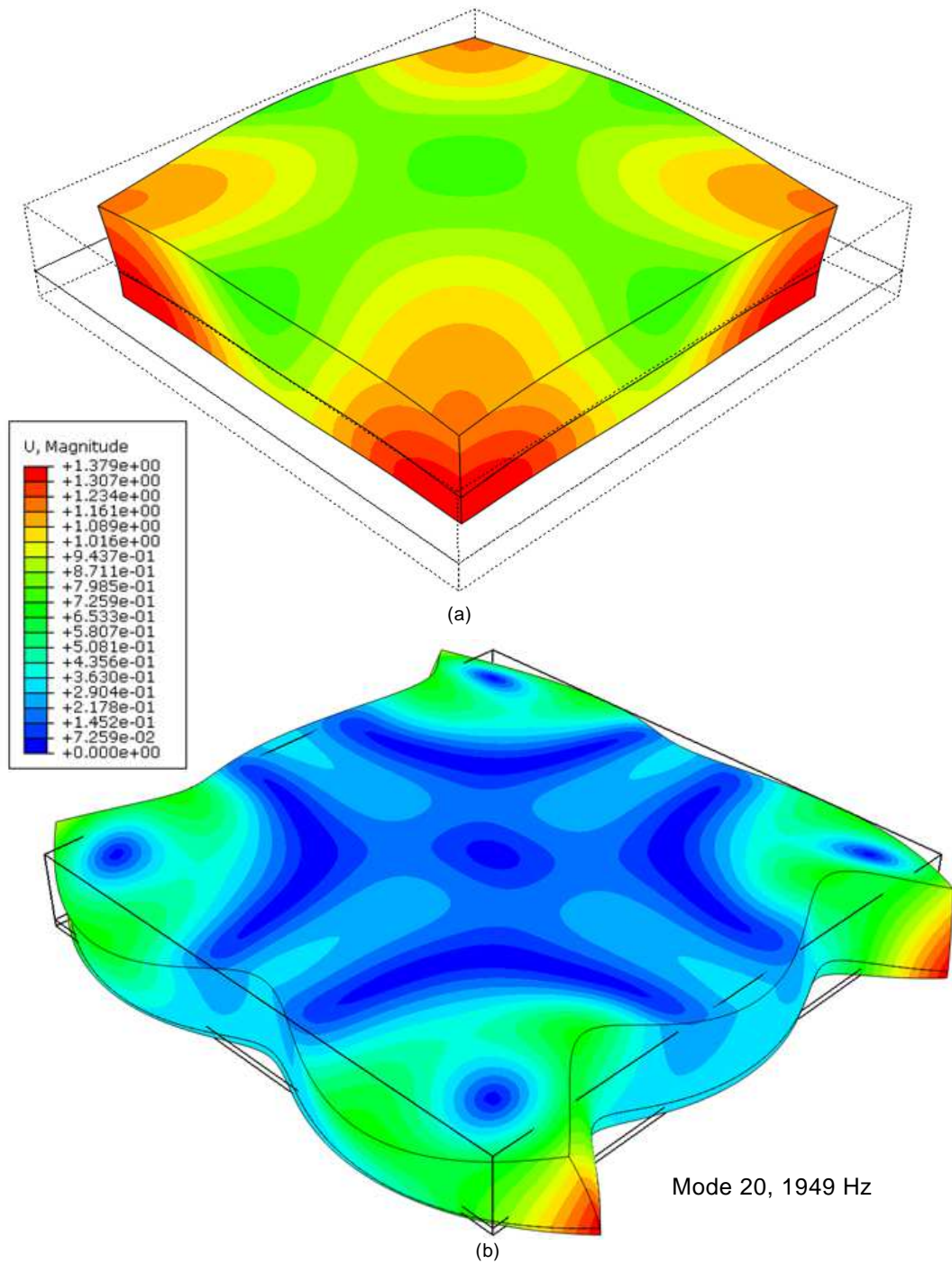
Figure 5.11   Results of Eigen-value analysis to determined the vibration

mode excited by the impact load for model: (a) M8, and (b) M3.

89

5.6 PLATE-FOUNDATION LAYER IMPEDANCE RATIO R_Z

Four simulations, namely M3, M9, M10 and M11 as listed in Table 5.7 were run to understand the effect of concrete-foundation impedance ratio on the propagating stress waves. The impedance ratios R_Z were taken as 34, 5886, 111 and 10.8 for M3, M9, M10 and M11 respectively as discussed in Section 4.2.5.2.

Table 5.8 summarizes the foundation layer material properties used in the models to attain the respective R_Z.

Figure 5.12 represents the displacement time-histories for these different cases. For models M3, M9, and M10, the compression incident wave was reflected back as tension wave at 2P while for M11, there was no phase change at the interface and the compression incident wave was reflected back as a compression wave at 2P (P represents the arrival of the first reflected P-wave at the impact surface, equal to 62 µs). Figure 5.13 compares the amplitude spectra for the different simulation cases. For models M3, M9 and M10, distinct peaks representing the thickness-mode frequency were identified whereas no such peak was observed for M11.

The varying elastic modulus of the foundation layer also affects the axial stiffness and hence the piston-mode frequency of the system. For M9, this frequency (approx. 13 Hz) was undetectable in the FFT plot at the standard frequency resolution. For M11, only one peak was observed at 3296 Hz which can be attributed to the concrete-plate assembly

90

vibrating in the same mode. Higher value of plate-foundation impedance ratio increases the accuracy of identification of distinct peak pertaining to thickness-mode frequency.

5.6.1 Summary

The ratio of the plate impedance to the foundation impedance R_Z influences the behavior of wave at the concrete/foundation layer interface. A higher R_Z will yield a higher coefficient of reflection R and therefore maximum of the incident wave will be reflected. Models with low value of R_Z produces erroneous frequency peaks and the thickness-mode frequency cannot be distinguished.

Table 5.7   Summary of analyses evaluated to study the effect impedance ratio.

ID	Force-time Function		Force Distribution		Impact Location			Boundary Condition			Foundation Layer Properties	
	HS	HSC	Point	Pressure	I_1	I_2	I_3	Clamped	ALID	Foundation Layer	R_K	R_Z
M3		✓		✓	✓					✓	1.16	34
M9		✓		✓	✓					✓	1.16	5886
M10		✓		✓	✓					✓	1.16	111
M11		✓		✓	✓					✓	1.16	10.8

Table 5.8   Table summarizing the FE models with varying impedance property of foundation layer.

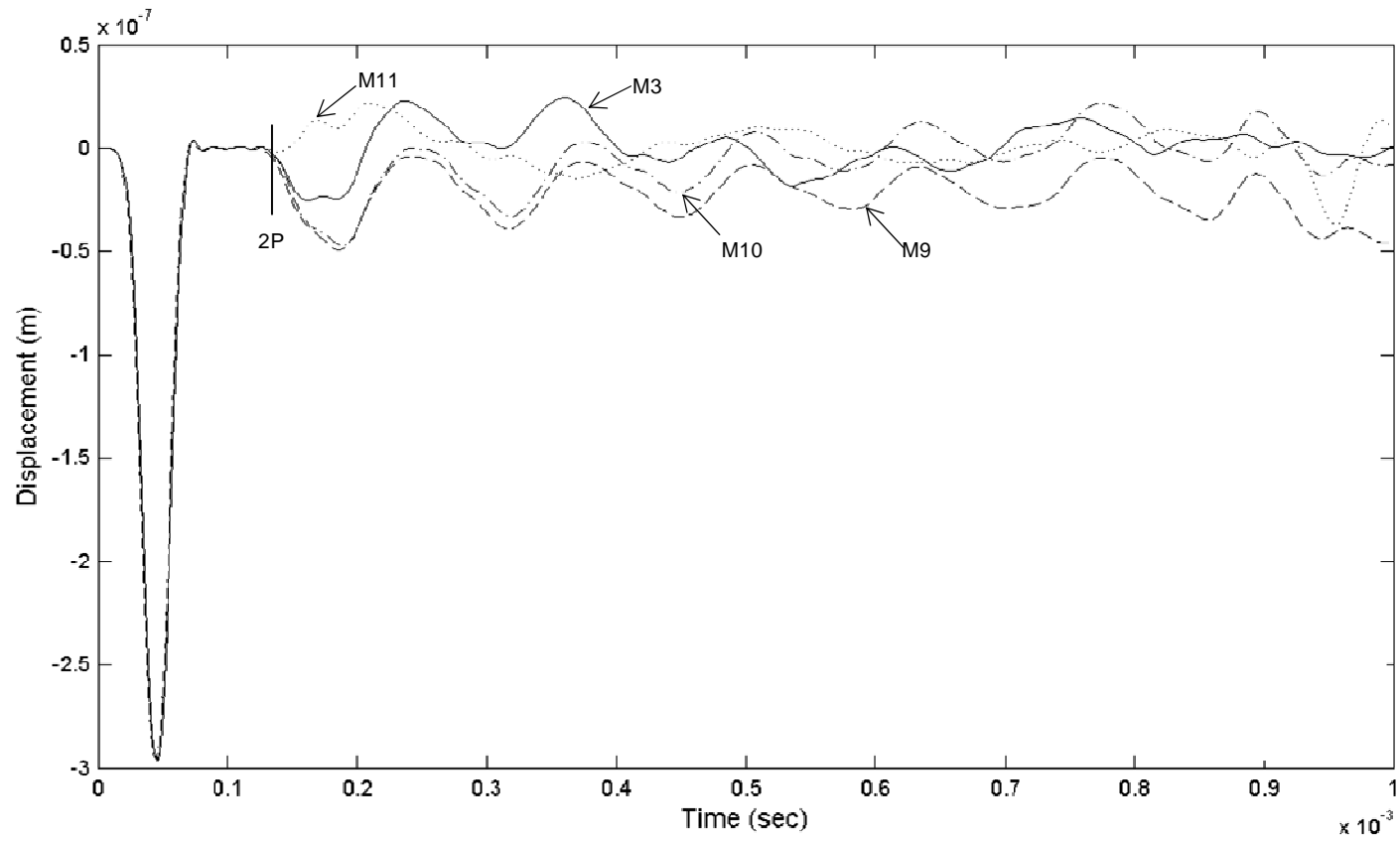| ID	Foundation Layer Properties				R_Z	Frequency			
	E	C_P	ρ	Z		f_{th}	f_T	f_P	f_{SDOF}
	(Pa)	(m/s)	(Kg/m^3)	(Kg/m^2 − s)		(Hz)	Hz	(Hz)	(Hz)
M9	$1{\times}10^5$	82	20	$1.6{\times}10^3$	5886	7568	7671	-	13
M10	$2{\times}10^8$	3101	28	$1{\times}10^5$	111.3	7568	7671	610	581.5
M3	$3{\times}10^9$	14210	20	$2.8{\times}10^5$	34	7813	7671	1953	2252
M11	$3{\times}10^{10}$	44940	20	$8.9{\times}10^5$	10.8	3296	7671	-	7121

Figure 5.12   Comparison of displacement time-history for models with varying acoustic impedances of foundation layer.
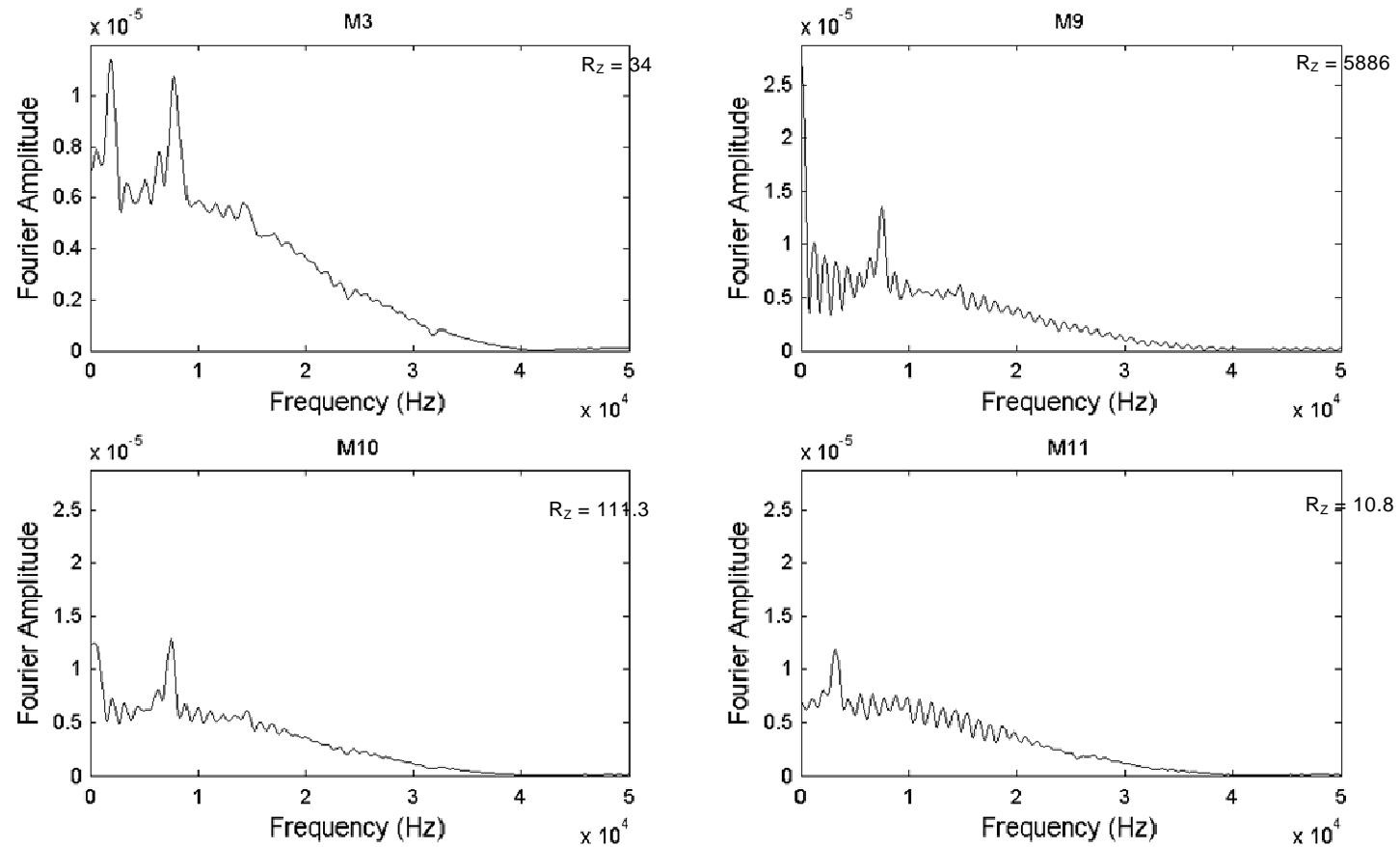
Figure 5.13   Comparison of amplitude spectra for models with varying impedances of foundation layer.

CHAPTER 6. SUMMARY, CONCLUSIONS AND FUTURE WORK

This chapter summarizes the current research investigation and draws significant conclusions based on the numerical simulation carried out to study wave propagation in concrete plates. At the end of this chapter potential future research topics are proposed that can be explored to extend the present study to evaluate more complex problems.

6.1 SUMMARY

This research investigates the numerical modeling of stress wave propagation in the concrete plates when impacted by a steel sphere. Various FE models were developed to study the wave propagation characteristics in bounded and semi-infinite plate sections. Dynamic analysis of the models was carried out using ABAQUS FE software.

The research was focused on developing a modeling methodology for the propagation of elastic stress wave in concrete for which different cases were analyzed. The impact of the force-time function defined by a half cycle sine and half cycle sine cubed function on the waveform was studied. The effect of the impact load applied on a single node vs distributed over several nodes was examined.

The efficacy of energy absorbing layer in attenuating the unwanted side reflections was examined by providing ALIDs at the boundaries of the area of interest. The damping was achieved by introducing mass proportional Rayleigh damping in the layer.

www.manaraa.com

A new modeling technique for the bounded concrete section was established by modeling a foundation layer to support the concrete slab. Parametric studies of individual material properties of the foundation layer were conducted to understand the importance of each property in determining the characteristics of the wave propagation.

6.2 CONCLUSIONS

Based on the results of the set of FE models that were investigated in the present study, the following conclusions and inferences were drawn:

1. The formulation of force-time function is important in determining the maximum frequency of useful energy. For the same contact time t_c and amplitude F_{max} half-cycle sine cubed (HSC) yields a higher maximum useful frequency than the half-cycle sine (HS).

2. Modeling the impact load by HS force-time function induces high frequency oscillations or "ringing" in the waveform. Using a more gradual slope to represent the force-time function can be used to eliminate the artificial ringing.

3. Localized deformation of the concrete surface takes place (represented by undulations in the displacement history) when the impact load is concentrated over a single node. This effect can be eliminated by modeling the impact load as a pressure load distributed over two or more nodes. However modeling the impact as concentrated load does not affect the accuracy of the thickness-mode frequency.

4. For a semi-infinite section, wave reflections from the clamped boundaries influence the displacement time-history and yield erroneous peak frequency in the amplitude spectrum. To avoid such discrepancies a sufficiently large model can be built to shun the effect of boundary reflections for the analysis time. This however adds extensively to the computational cost. The same effect can also be achieved by using non-reflecting or absorbing boundaries.

5. A significant reduction in model's geometric size and computational cost can be achieved by implementing the absorbing layer with increased damping (ALID) boundary condition. While modeling the ALID boundaries, the length L_D and the mass proportion Rayleigh damping coefficient C_M affects it efficiency in attenuating the amplitude of the propagating wave.

6. The foundation layer approach was successfully applied to study the wave propagation in concrete plates of a finite dimension. The amplitude spectrum of the system consisting of a concrete plate supported on flexible foundation layer is dominated by the piston-mode and thickness-mode frequencies.

7. Concrete plate supported on flexible foundation layer behaves as a rigid mass supported on soft spring and vibrates in piston-mode that is easily detected in the amplitude spectrum as a distinct peak. This mode of vibration can also be estimated by calculating the fundamental frequency of a SDOF model comprising rigid mass (equal to mass of concrete plate) supported on a spring of stiffness K_f (axial stiffness of foundation layer).

8. The ratio of the plate stiffness to the foundation layer stiffness R_K determines the piston-mode frequency of concrete-foundation layer assembly. A higher value of

97

R_K, that represents a more flexible foundation layer, improves the accuracy of the amplitude spectrum in distinguishing the thickness-mode and piston-mode frequency. A stiffer foundation layer possesses ambiguity in distinguishing the thickness-mode frequency from the amplitude spectrum.

9. The ratio of the plate impedance to the foundation impedance R_Z influences the behavior of wave at the concrete/foundation layer interface. A higher R_Z will yield a higher coefficient of reflection R and therefore maximum of the incident wave will be reflected. Models with low value of R_Z produces erroneous frequency peaks and the thickness-mode frequency cannot be distinguished.

10. For the concrete plate with foundation layer boundary condition, eccentric impact loading does not excite any higher flexural mode other than the piston-mode of the foundation layer. However, the displacement histories for eccentric deviates from that of symmetric loading at around 5P owing to the early arrival of the P-waves reflected from the free boundary of the concrete plate. This deviation becomes profound at around 10P during which the side wave reflections increases.

6.3 FUTURE WORK

The scope of the current research is limited to simple square plate geometry that is free from any internal defects. Moreover, all the simulations and observations are specific to plates of thickness of 0.25 m. The present research can be extended to provide modeling basis for thin and deeper generalized sections. Following future research topics are proposed to support the current project:

98

1. Study the wave propagation characteristics in presence of complex defects such as surface opening cracks, voids, delamination, partially grouted cracks, etc.

2. Study the transient response of concrete plate in contact with steel plate, soil, rock etc. and analyze the influence of the underlying material on the identification of thickness-mode frequency.

3. Study the accuracy of the foundation layer approach in isolating the piston-mode and thickness-mode frequencies for a reduced area of concrete plate.

4. Conduct a comparative analysis to study the effectiveness of the foundation layer in comparison to other absorbing boundaries such perfectly matched layer (PML), Lysmer-Kuhlemeyer (LK) boundaries, etc.

REFERENCES

ABAQUS. (2011). *ABAQUS Documentation.* Providence, RI, USA: Dassault Systèmes.

Abramo, D. (2011). *Impact-Echo Modeling and Imaging Techniques.* Doctoral dissertation, Northeastern University.

Bathe, K. J. (1996). *Finite element procedures.* Prentice Hall.

Berenger, J. P. (1994). A perfectly matched layer for the absorption of electromagnetic waves. *Journal of Computational Physics, 114*(2), 185-200.

Brekhovskikh, L. (2012). *Waves in Layered Media 2e* (Vol. 16). Elsevier.

Carino, N. J. (2001). The impact-echo method: an overview. *In Proceedings of the 2001 Structures Congress & Exposition* (pp. 21-23). Washington, DC: American Society of Civil Engineers.

Chang, H. W., & Randall, C. J. (1988). Finite-difference time-domain modeling of elastic wave propagation in the cylindrical coordinate system. *In Ultrasonics Symposium, 1988. Proceedings* (pp. 397-402). IEEE.

Chopra, A. K. (1995). *Dynamics of structures* (Vol. 3). New Jersey: Prentice Hall.

100

Davis, A. G., Gaynor, R. D., Lozen, K. M., Rowe, T. J., Caratin, H., ..., & Sansalone, M.
J. (1998). Nondestructive Test Methods for Evaluation of Concrete in Structures.
American Concrete Institute, ACI, 228.

Drozdz, M. B. (2008). *Efficient Finite Element modelling of ultrasound waves in elastic
media* . Doctoral dissertation, Imperial College London.

Gibson, A., & Popovics, J. S. (2005). Lamb wave basis for impact-echo method analysis.
Journal of Engineering Mechanics, 4(131), 438-443.

Goldsmith, W. (1960). *Impact: the theory and physical behaviour of colliding solids.*
London: Edward Arnold .

Graff, K. F. (1975). *Wave motion in elastic solids.* Courier Dover Publications.

Guide, M. U. (1998). *The mathworks* (Vol. 5). Natick, MA: Inc.

Ham, S., & Bathe, K. J. (2012). A finite element method enriched for wave propagation
problems. *Computers & Structures, 94*, 1-12.

Hunter, S. C. (1957). Energy absorbed by elastic waves during impact . *Journal of the
Mechanics and Physics of Solids, 5*(3), 162-171.

Lamb, H. (1904). On the propagation of tremors over the surface of an elastic solid .
*Philosophical Transactions of the Royal Society of London. Series A, Containing
Papers of a Mathematical or Physical Character*, 1-42.

101

Lamb, H. (1917). On waves in an elastic plate. *Proceedings of the Royal Society of London. Series A, Containing papers of a mathematical and physical character*, (pp. 114-128).

Lin, Y., & Sansalone, M. (1992). Transient response of thick circular and square bars subjected to transverse elastic impact. *The Journal of the Acoustical Society of America, 91*(2), 885-893.

Lin, Y., & Sansalone, M. (1992). Transient response of thick rectangular bars subjected to transverse elastic impact. *The Journal of the Acoustical Society of America, 91*(5), 2674-2685.

Lysmer, J., & Kuhlemeyer, R. (1969). Finite dynamic model for infinite media. *Journal of the Engineering Mechnanics Division, Proc. ASCE, 95*, pp. 859 – 876.

McLaskey, G. C., & Glaser, S. D. (2010). Hertzian impact: experimental study of the force pulse and resulting stress waves. *The Journal of the Acoustical Society of America, 128*(3), 1087-1096.

Miklowitz, J. (1984). *The theory of elastic waves and waveguides.* Elsevier.

Miller, G. F., & Pursey, H. (1954). The field and radiation impedance of mechanical radiators on the free surface of a semi-infinite isotropic solid. *Proceedings of the Royal Society of London. Series A. Mathematical and Physical Sciences, 223*(1155), 521-541.

Miller, G. F., & Pursey, H. (1955). On the partition of energy between elastic waves in a semi-infinite solid. *Proceedings of the Royal Society of London. Series A. Mathematical and Physical Sciences, 233*(1192), 55-69.

Oh, T. K. (2012). *Defect characterization in concrete elements using vibration analysis and imaging*. Doctoral dissertation, University of Illinois at Urbana-Champaign.

Ohtsu, M., & Watanabe, T. (2002). Stack imaging of spectral amplitudes based on impact-echo for flaw detection. *NDT & E International, 35*(3), 189-196.

Olsson, D. (2012). *Numerical simulations of energy absorbing boundaries for elastic wave propagation in thick concrete structures subjected to impact loading.* Thesis, Umeå University.

Pessiki, S. P., & Carino, N. J. (1988). Setting time and strength of concrete using the impact-echo method. *ACI Materials Journal, 85*(5), 389-399.

Pessiki, S., & Johnson, M. R. (1996). Nondestructive evaluation of early-age concrete strength in plate structures by the impact-echo method. , 93(3). *ACI Materials Journal, 93*(3), 260-271.

Pessiki, S., & Rowe, M. H. (1997). Influence of steel reinforcing bars on the evaluation of early-age concrete strength using the impact-echo method. *ACI structural journal, 94*(4), 378-388.

103

Rayleigh, L. (1888). On the free vibrations of an infinite plate of homogeneous isotropic elastic matter. *Proceedings of the London Mathematical Society, 1*(1), 225-237.

Sansalone, M., & Carino, N. J. (1986). *Impact-echo: a method for flaw detection in concrete using transient stress waves.* US Department of Commerce, National Bureau of Standards, Center for Building Technology, Structures Division.

Sansalone, M., & Street, W. (1997). *Impact-echo: nondestructive evaluation of concrete and masonry.* Bullbrier Press.

Sansalone, M., Carino, N. J., & Hsu, N. N. (1987). A finite element study of transient wave propagation in plates. *NBS Journal of Research, 92*(4).

Schubert, F., & Köhler, B. (2008). Ten lectures on impact-echo. *Journal of Nondestructive Evaluation, 27*(1-3), 5-21.

Schubert, F., Wiggenhauser, H., & Lausch, R. (2004). On the accuracy of thickness measurements in impact-echo testing of finite concrete specimens—numerical and experimental results. *Ultrasonics, 42*(1), 897-901.

Seron, F. J., Sanz, F. J., Kindelan, M., & Badal, J. I. (1990). Finite-element method for elastic wave propagation. *6*(5), 359-368.

Thomson, W. T. (1950). Transmission of elastic waves through a stratified solid medium. *Journal of applied Physics, 21*(2), 89-93.

Timoshenko, S. P., Goodier, J. N., & Abramson, H. N. (1970). Theory of elasticity. *Journal of Applied Mechanics, 37*, 888.

Viktorov, I. A. (1967). *Rayleigh and Lamb waves: physical theory and applications* (Vol. 147). New York: Plenum press.

Woods, R. D. (1968). *Screening of surface waves in soil.* University of Michigan.

Zhang, Y., Wei, X., Tsai, Y. T., Zhu, J., Fetrat, F. A., & Gucunski, N. (2012). Multisensor data fusion for impact-echo testing of concrete structures. *Smart Materials and Structures, 21*(7), 075021.

VITA

Tripti Pradhan was born on 19th June 1988 in the Himalayan state of Sikkim in India. She is the youngest child of Mr. Tara K. Pradhan and Ms. Bishnu Pradhan. She completed her high school education from Holy Cross School, Tadong in the year 2006. She received her Bachelors of Technology degree in Civil Engineering in June 2010 from G. B. Pant University of Agriculture and Technology. She then worked as a Research Project Associate at Indian Institute of Technology Kanpur for approximately two years and pursued research under the guidance of Dr. Durgesh C. Rai. She started her graduate studies with the Department of Civil and Environmental Engineering at Lehigh University in August 2012 and expects to complete M.S. in Structural Engineering in December 2014.

List of Publications

Rai, D. C., Annam, P. K., & Pradhan, T. (2013). Seismic testing of steel braced frames with aluminum shear yielding dampers. *Engineering Structures*, *46*, 737-747.

Rai, D. C., Mondal, G., Singhal, V., Parool, N., Pradhan, T., & Mitra, K. (2012). Reconnaissance report of the M6. 9 Sikkim (India–Nepal border) earthquake of 18 September 2011. *Geomatics, Natural Hazards and Risk*, *3*(2), 99-111.

Rai, D. C., Komaraneni, S., & Pradhan, T. (2011). Strengthening of Slab Action in Transverse Direction of Damaged Deck of Prestressed Box Girder Bridge. *Journal of Bridge Engineering*, *18*(1), 65-75.